CALIBRATION OF A NaI (Tl) DETECTOR FOR LOW LEVEL COUNTING OF NATURALLY OCCURRING RADIONUCLIDES IN SOIL

Sive Professor Noncolela

Thesis presented in fulfilment of the requirements for the degree of
Magister Scientiae at the University of the Western Cape

Supervisor: Prof. R Lindsay
Physics department
University of the Western Cape

November 2011

CALIBRATION OF A NaI (Tl) DETECTOR FOR LOW LEVEL COUNTING OF NATURALLY OCCURRING RADIONUCLIDES IN SOIL

Sive Professor Noncolela

Keywords

Activity Concentration
Background radiation
Calibration
Full Spectrum Analysis
^{40}K
Least Squares Method
Low Level Counting
Matlab
Mine dumps
Spectral drift
^{232}Th
^{238}U

DECLARATION

I, the undersigned, declare that the work contained in this thesis is my own original work and that I have not previously in its entirety or in part submitted it to any university for a degree.

Signature:……

Date:……..

CALIBRATION OF A NaI (Tl) DETECTOR FOR LOW LEVEL COUNTING OF NATURALLY OCCURRING RADIONUCLIDES IN SOIL

Sive Professor Noncolela

Abstract

The Physics Department at the University of the Western Cape and the Environmental Physics group at iThemba labs have been conducting radiometric studies on both land and water. In this study a 7.5 cm X 7.5 cm NaI (Tl) detector was used to study activity concentrations of primordial radionuclides in soil and sand samples. The detector and the sample were placed inside a lead castle to reduce background in the laboratory from the surroundings such as the wall and the floor. The samples were placed inside a 1 L Marinelli beaker which surrounds the detector for better relative efficiency as almost the whole sample is exposed to the detector. Additional lead bricks were placed below the detector to further reduce the background by 20%. The NaI detector is known to be prone to spectral drift caused by temperature differences inside and around the detector. The spectral drift was investigated by using a ^{137}Cs source to monitor the movements in the 662 keV peak. The maximum centroid shift was about 4 keV (for a period of 24 hours) which is enough to cause disturbances in spectral fitting. There was no correlation between the centroid shift and small room temperature fluctuations of 1.56 ºC.

A Full Spectrum Analysis (FSA) method was used to extract the activity concentrations of ^{238}U, ^{232}Th and ^{40}K from the measured data. The FSA method is different from the usual Windows Analysis (WA) as it uses the whole spectrum instead of only putting a 'window' around the region of interest to measure the counts around a certain energy peak. The FSA method uses standard spectra corresponding to the radionuclides being investigated, and is expected to have an advantage when low-activity samples are measured. The standard spectra are multiplied by the activity concentrations and then added to fit the measured spectrum. Accurate concentrations are then extracted using a chi-squared (χ^2) minimization procedure.

Eight samples were measured in the laboratory using the NaI detector and analyzed using the FSA method. The samples were measured for about 24 hours for good statistics. Microsoft Excel and MATLAB were used to calculate the activity concentrations. The ^{238}U activity concentration values varied from 14 ± 1 Bq/kg (iThemba soil, HS6) to 256 ± 10 Bq/kg (Kloof sample). The ^{232}Th activity concentration values varied from 7 ± 1 Bq/kg (Anstip beach sand) to 53 ± 3 Bq/kg (Rawsonville soil #B31). The ^{40}K activity concentration values varied from 60 ± 20 Bq/kg (iThemba soil, HS6) to 190 ± 20 Bq/kg (Kloof Sample). The χ^2 values also varied from sample to sample with the lowest being 12 (Anstip beach sand) and the highest (for samples without contamination of anthropogenic nuclei) being 357 (Rawsonville soil #B28). A high χ^2 value usually represents incomplete gain drift corrections, improper set of fitting functions, proper inclusion of coincidence summing or the presence of anthropogenic (man made) radionuclei in the source [Hen03].

Activity concentrations of ^{40}K, ^{232}Th and ^{238}U were measured at four stationary points on the Kloof mine dump. The fifth stationary point was located on the Southdeep mine dump. These measurements were analysed using the FSA method and fitting by "eye" the standard spectra to the measured spectra using Microsoft Excel. These values were then compared to values obtained using an automated minimisation procedure in MATLAB. There was a good correlation between these results except for ^{232}Th which had higher concentrations when MATLAB was used, where 16 Bq/kg was the average value in Excel and 24 Bq/kg was the average value in MATLAB.

DEDICATION

To:

1. The memory of my late grandparents Ernest and Angelina Noncolela, who planted the seed of education in our family despite themselves being illiterate. Ndiyabulela Deyi nawe Bhelekazi.

2. The memory of my late grandmother Nomakhulu Novukela, who supported me during my undergraduate years. Ndiyabulela maJili noba awuzibonanga iziqhamo zomsebenzi wakho.

ACKNOWLEDGEMENTS

I would like to show my sincere gratitude to the following people:

- **Prof. Robbie Lindsay**, supervisor, for his guidance, support and active involvement in challenging aspects of my thesis.

- **Dr. Richard Newman,** who gave permission to use the equipment in the **Environmental Research Laboratory** at **iThemba LABS**. I am also grateful for his support and helpful suggestions.

- **Prof. Rob de Meijer, Dr Peane Maleka** and **Dr Siddig Talha,** for helpful discussions and moral support.

- **Prof. Chris Koen** for helpful discussions on data analysis and Matlab.

- Former and current colleges at UWC and ERL such as **Israel Hlatshwayo, Nolasco Mlwilo, Joash Ongori, Johann Mvelase, Andrew Esau, Tshepo Dinoko, Thobeka Wittes,** for advice, suggestions and encouragement.

- **NRF** and **iThemba LABS**, for financial and technical support.

- **Mr Ian Schroeder, Mrs Angela Adams and the rest of the staff at Physics department at UWC**, for their warm welcome and the opportunity to be part of the **MANUS/MatSci** programme and for all the support.

- **Mr Zama Zituta** and Goldfields Co. for allowing us to take measurements at the Kloof mine and for giving us the support we needed.

- My parents, **Soldati no Faniswa Noncolela** ngokundithanda, ndindikhulise, nindifundise. Ndiyabulela **Deyi** nawe **maJili/maZulu**, abekho abazali abadlula nina. To my sister **Zimasa**, ndiyabulela kakhulu ngokusoloko undinceda, undixhasa. To the rest of my siblings, **Siphelele**, **Sisonke** and **Anazi** ndiyathemba ukuba nani nizokhuthazeka, nifunde, niphumelele. Ndiyabulela nakusapho lonke lwama**Deyi** nezihlobo.

- Ekugqibeleni ku**Mdali** wezinto zonke. Thank you **Heavenly Father** for being with me at all times.

Table of Contents

Appendices:

List of Figures

List of Tables

Chapter 1 Introduction

Terrestrial radiation has been around since the creation of the earth's crust. It is found in rocks, soil, air, water and vegetation. Since human beings are always in contact with the above sources of terrestrial radiation it is therefore important to measure them and know how they influence our daily lives. In this chapter a brief history of the NaI detector and the early discovery of the nucleus is discussed, followed by the motivation and the scope of the study.

The NaI(Tl) is an inorganic scintillator that was discovered by Robert Hofstadter in 1948 [Kno00]. It has been used since the beginning of gamma spectroscopy and it is still one of the most utilised detectors today. It is widely used because of the fact that it is a relatively cheap detector but with many advantages. It has high intrinsic efficiency compared to semiconductor detectors and most scintillators (BGOs are more efficient, but suffer from poorer resolution). It has the greatest light output among the scintillators and hence good resolution [Gil95]. It has some drawbacks though as it is a brittle crystal which is also hygroscopic so care should be exercised in handling it and it must be enclosed at all times. It is also not suitable for fast timing or high counting rate applications as it has a long decay time of scintillazation pulse (about 230 ns) and undesirable phosphorescence (afterglow) [Kno00].

High Purity Germanium (HPGe) detectors are often used in the study of natural radioactivity in soil [Map04]. This is because of the detector's resolution abilities. It is however also known that HPGe detectors are not the most efficient detectors at least not better than NaI (Tl). This fact makes NaI (Tl) detectors better suited for low level counting than HPGe detectors especially if the radionuclides being investigated are known and so the energy resolution capabilities are not critical.

The study of naturally occurring radioactive material (NORM) has had many applications from mining, agriculture and other environmental measurements. These measurements require a precise and accurate measurement of activity concentrations of these NORMs. A better method to the traditionally used windows analysis has been developed for activity concentration measurements. This full spectrum analysis method (FSA) has been developed to obtain more precise and accurate measurements than the windows analysis method [Hen01], [Hen03].

A combination of a high efficient detector and a reliable method has led to this study, to see whether the NaI (Tl) detector can be used for low level counting combined with a full spectrum analysis method.

1.1 Early discoveries and the nucleus

In 1896 Henri Becquerel encountered radiation by chance when he observed that uranium salts emitted radiations capable of affecting a photographic plate. This was two years after the discovery of X-rays by Roentgen. A few years later Marie and Pierre Curie discovered two other substances which were more active than uranium, namely polonium (Po) and radium (Ra) which they isolated from a uranium ore [Lap72].

In 1932 James Chadwick proposed the existence of an uncharged nuclear constituent which was named a neutron. This was after F Joliot an I Curie measured fast protons emerging from paraffin exposed to a highly penetrating uncharged radiation from the a bombardment of beryllium. Chadwick correctly predicted the mass of a neutron from the recoils of proton and nitrogen from different bombardment materials. He found the mass of the neutron to be approximately that of a proton [Lil01].

The nucleus of an atom is made up of a certain number of protons (Z) and a certain number of neutrons (N). The assembly of nucleons with their associated electrons are referred to as a nuclide and hence called radioactive nuclides when they are radioactive. Elements can have the same Z and different N making them isotopes and hence called radioactive isotopes when they undergo radioactive decay [Gil95]. The complicated nuclear interactions between protons and neutrons lead to some nuclei which have very long half lives which may decay naturally by α, β and ɣ decay, allowing us to measure the concentrations of these elements.

1.2 Motivation for this study

South Africa as a country is known for being a mining country, it is a leader in production of platinum, manganese, chrome and vanadium and ranks second in gold, zirconium and titanium production [www01]. Most minerals being mined come from rocks which contain radioactive elements. This has made radiometric studies in the work and outside environment important in addressing these radioactive nuclides as a potential health hazard and for exploration reasons.

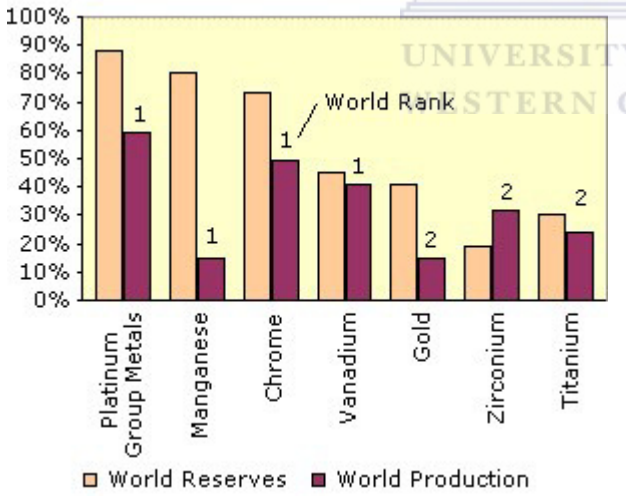

Figure 1.1: A graphical representation of South Africa's share in world production and reserves [www01]. The numbers indicate South Africa's ranking in world production.

Some studies have been conducted already by de Meijer [Dem98] in what is called radiometric fingerprinting. The study was conducted around the coast of SA as shown in figure 1.2 including regions where there are activities of dune mining. Namakwa Sands is one of the companies where heavy minerals like zirconium are mined from the dune sands. These mineral sands have been found to contain natural radioactive particles like ^{238}U, ^{232}Th and ^{40}K in large concentrations.

Detection of these gamma ray emitting nuclides can lead to a faster way of locating these minerals rather than determining the heavy-mineral content by floating them off in heavy minerals, for example [Dem98].

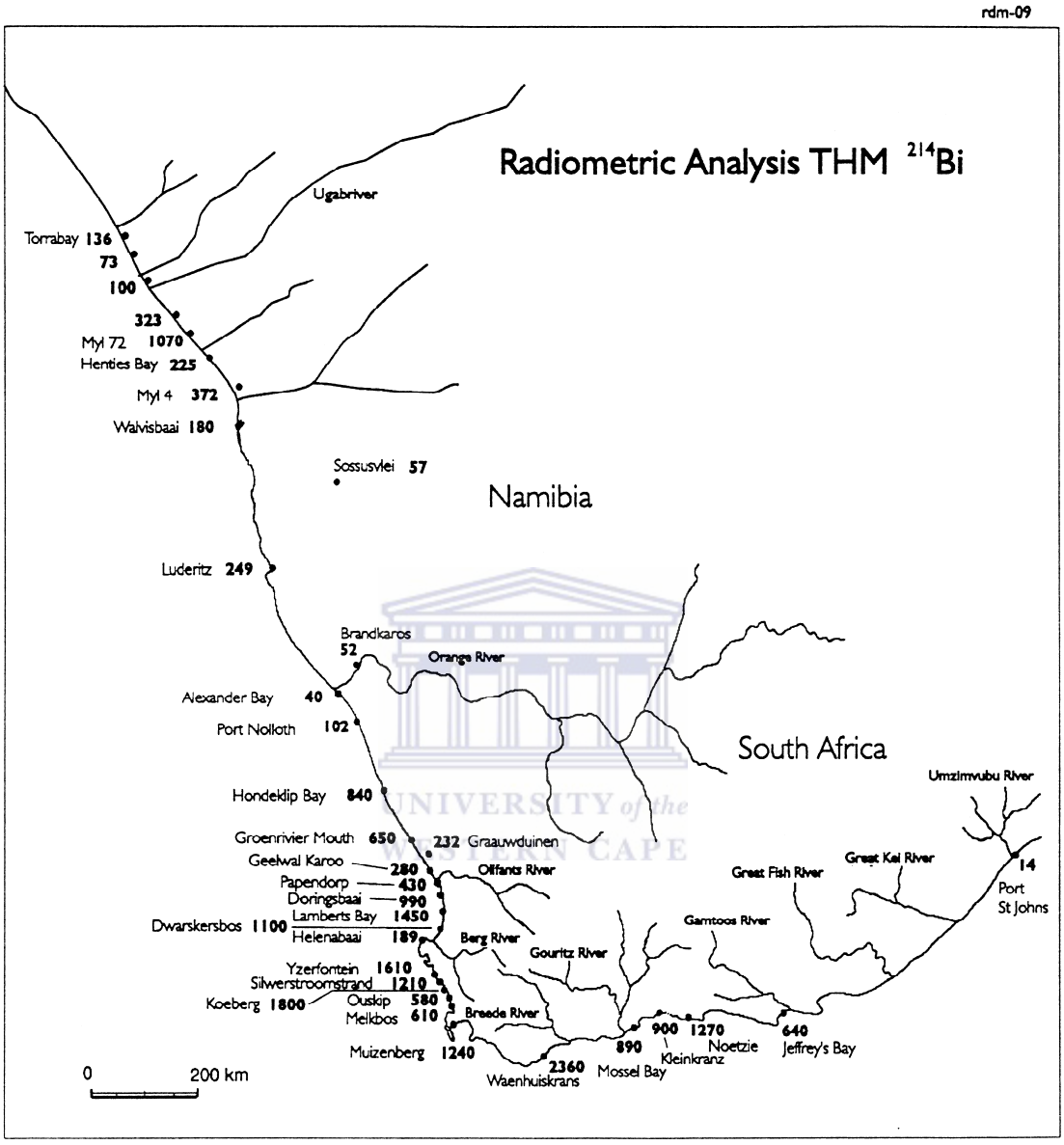

Figure 1.2: A figure showing the Activity Concentration (Bq/kg^{-1}) [Total Heavy-mineral Mass (THM) content] of ^{214}Bi in the heavy mineral fraction of sand samples in South Africa and Namibia [Dem98].

Some studies have also been done in mine dumps for health reasons [Lin04]. Again these studies have been made possible by gamma spectrometry of ^{238}U, ^{232}Th, progenies and ^{40}K with the exhalation of ^{222}Rn (radon) in particular being the main health concern. The spillage of the radioactive nuclides to the surrounding environment and the ecosystem is also a concern in these mine tailings.

There is a need for further improvements in measurements and detection methods in these areas. There is also a need to optimize our detectors for best measurements by improving both the hardware setup and software for detection. For this to happen our detectors should be calibrated correctly and its sensitivity be compared to other detectors that are available.

1.3 Scope of the study

The partnership of the physics department at the University of the Western-Cape (UWC) and iThemba LAB's Environmental Radiation Laboratory (ERL) has led to many studies in the field of environmental radiation. There is an abundance of detectors and detection systems from Rad 7 to Eperms, NaI, HPGe and Medusa. This thesis focuses on the calibration of a 7.5 cm X 7.5 cm NaI (Tl) detector for measurements of low level naturally occurring radionuclides like ^{238}U, ^{232}Th and ^{40}K. The NaI (Tl) detector does not have the good resolution of the HPGe, but is a much cheaper detector which can nevertheless provide good results in a shorter period due to its higher efficiency.

The radionuclides interact with the detector by gamma interactions that are described in chapter 2. The detector's response to these interactions is what enables us to measure the radiation emitted by the nuclides of interest and hence we can find their activity concentration and other information about the nucleus. The way in which these radioactive nuclides decay is also discussed in chapter 2.

In order to achieve the best results possible the detection setup should reduce interference from other sources of radiation. In chapter 3 the detection system setup is explained in detail in order to achieve good results. In conjunction with a good experimental setup should be a software and results analysis method. Chapter 3 also gives details of the data analysis. The FSA method is explained in depth in chapter 3. One of the disadvantages of the NaI (Tl) detector is the centroid drift associated with the detector. This has been investigated in this study and is discussed in chapter 4.

Soil and sand samples from different places were measured in the laboratory. They all gave different and interesting results which are discussed in chapter 4. Since most of the samples had low levels of radiation, minimising the background from the building materials was important. Results were achieved for the minimum detection level possible with the available equipment. The conclusion of the results is given in chapter 5 and also some outlook into future activities.

Chapter 2 Background theory: Natural radiation measurements

Gamma ray spectroscopy is made possible by the fact that the gamma rays from the decay of radioactive nuclides deposit some of their energy to the detector. Gamma rays emitted by these radionuclides interact with detecting material mostly by three ways described in this chapter. Gamma rays are not the only form of decay but they are the most important for our purpose because of their penetration depth as they travel further than betas and alphas. The decay chains of the three main naturally occurring radionuclides; ^{238}U, ^{232}Th and ^{40}K are discussed in detail in this chapter and finally a brief description on how the detector responds to the energy deposited by radionuclides.

2.1 Gamma ray interactions

Gamma rays are photons and the way they interact with matter is different from charged particles as they do not have an electric charge that creates many inelastic collisions with atomic electrons [Leo87]. If we consider the detector material as any piece of matter with gamma rays incident on it, the main types of interaction will be photoelectric absorption, Compton scattering and pair production.

2.1.1 Photoelectric absorption

One of the ways in which photons interact with matter is by photoelectric absorption. This is when a gamma ray photon impinges on an orbital electron in an atom and deposits all its energy to it. The electron is then ejected with energy

$$E_e = E_\gamma - E_b \qquad (2.1)$$

where E_e is the energy of the ejected electron (now called photoelectron), E_γ (= hν) being the energy of the impinging gamma-ray photon and E_b is the binding energy of the electron. For photoelectric absorption to take place the incident gamma-ray photon must have $E_\gamma \geq E_b$ which is usually the case. This process then leaves the atom in an excited state and it de-excites by occasionally releasing an electron of lower energy called an Auger electron but usually a higher orbital electron fills the gap left by the photoelectron and this could lead to an X-ray being emitted. Photoelectric absorption involves an orbital electron rather than a surface electron as both energy and momentum have to be conserved (free electrons cannot absorb a photon and recoil) [Kra88] as illustrated in figure 2.1. The kinetic energy K_e that the photoelectron leaves with is proportional to the energy of the impinging photon, hence equation 2.1 can also be written as

$$K_e = h\nu - E_b \qquad (2.2)$$

The energy of the incident gamma-ray and the atomic number of the absorbing material are the two most important factors to be considered for photoelectric absorption since the probability for photoelectric absorption to take place is given by

$$\sigma_{pe} \propto Z^n / E_\gamma^{3.5} \qquad (2.3)$$

where Z is the atomic number of the absorbing atom and n is between 4 and 5 for gamma ray energies E_γ of a few hundred keV [Lil01].

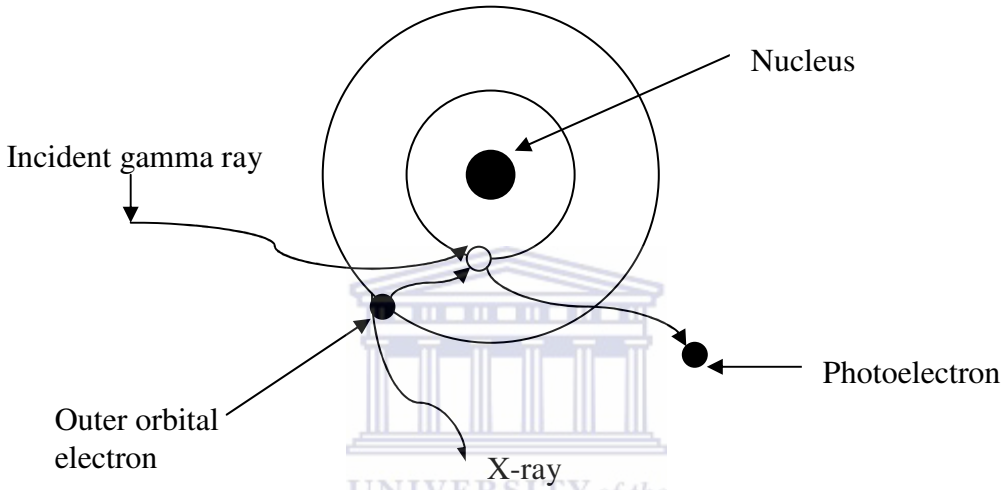

Figure 2.1: An incident gamma ray of energy E_γ ejects an inner-orbital electron and outer-orbital electron fills the vacant space and the atom de-excites by emitting an X-ray.

The energy dependence of the three modes of interaction for a gamma ray incident on a NaI detector are shown in figure 2.2 and 2.5 with low energies favouring photo electric absorption. High energy favours pair production whilst Compton scattering dominates in the middle.

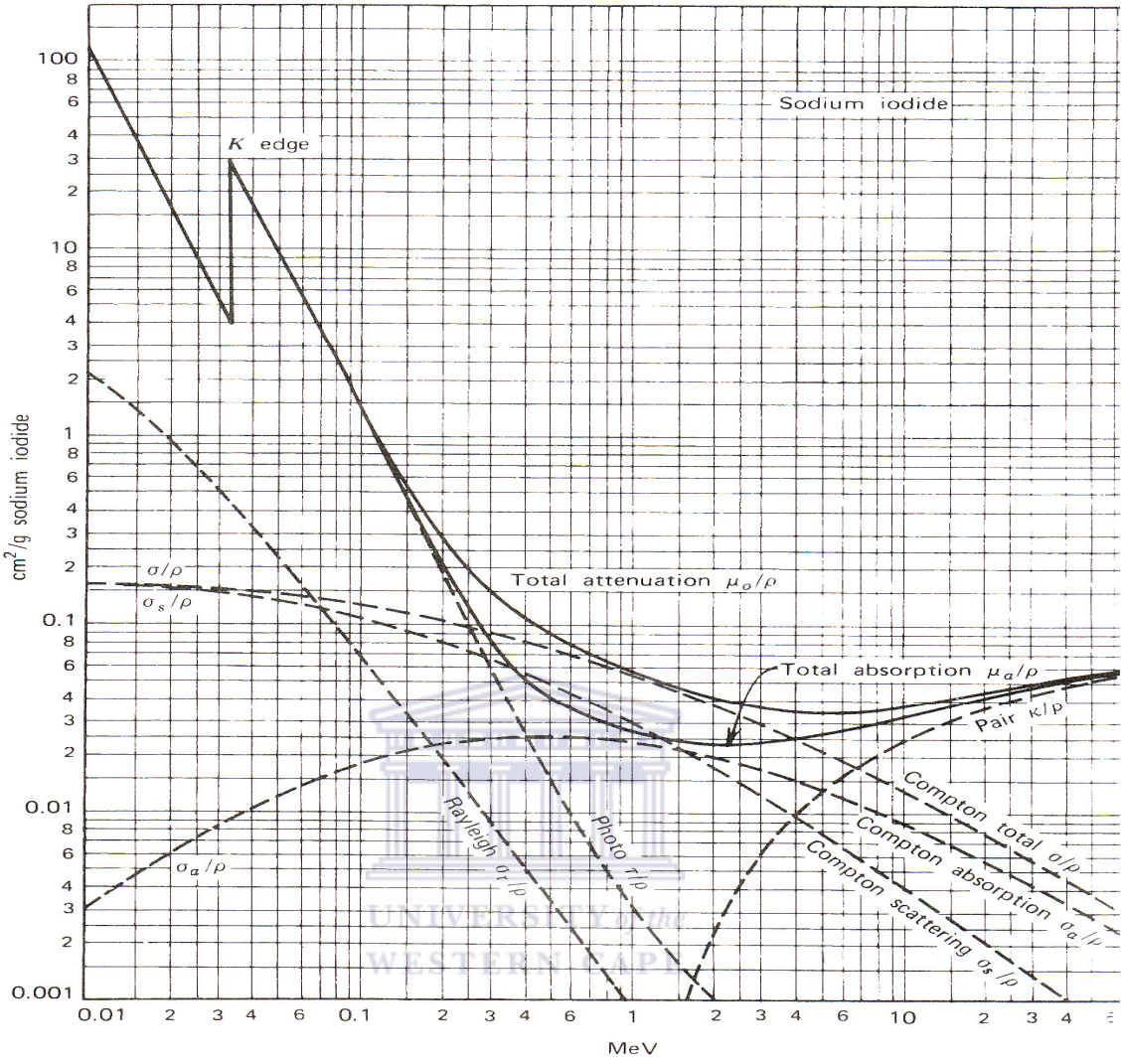

Figure 2.2: Illustration of the mass absorption coefficients for the photoelectric (τ/ρ), Compton (σ/ρ) and pair production (κ/ρ) interaction for NaI where ρ is the density. The total attenuation (μ_o/ρ) and absorption (μ_a/ρ) are also shown. [Kno00].

2.1.2 Compton Scattering

In 1923 Arthur H Compton discovered another way in which radiation interacts with matter when a beam of X-rays was scattered off a carbon target. This interaction is what is now known as Compton scattering. An incoming photon, in our case a gamma-ray, scatters off an "unbound" or almost "free" electron. It deposits some of its energy to this electron which then recoils. This means that the photon's initial energy is shared by the scattered photon and the recoiling electron. Both the scattered photon and electron are scattered at some angle relative to the incident photon and both momentum and energy are conserved in this scattering process [Kra83] as shown in figure 2.3.

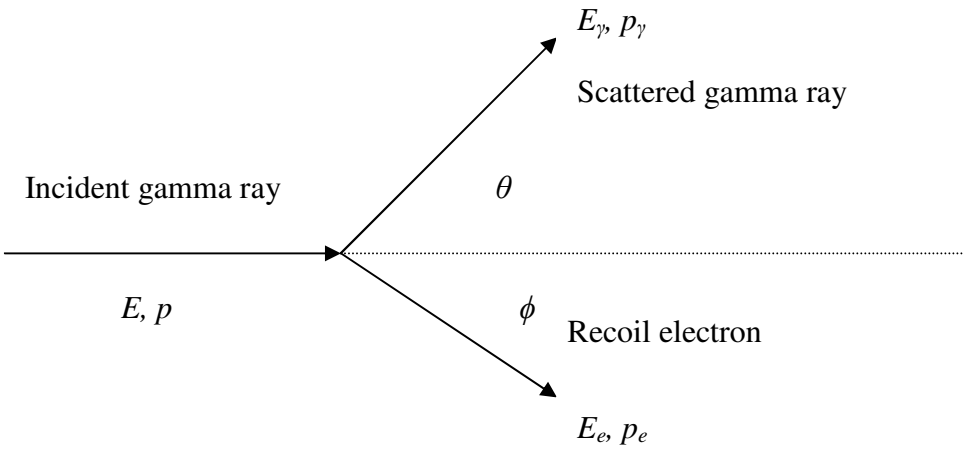

Figure 2.3: An example of a Compton scattering process where a scattered photon and electron share the energy from the incident photon.

The incoming photon will have energy equal to

$$E = E_\gamma + E_e \tag{2.4}$$

where E_γ is the energy of the scattered gamma ray photon and E_e is the energy of the scattered electron. Momentum of the incoming gamma ray photon is also expressed in terms of the momentum of the scattered photon and electron as

$$p = p_e \cos\phi + p_\gamma \cos\theta \tag{2.5}$$

in the direction of the incident gamma ray photon and

$$0 = p_e \sin\phi - p_\gamma \sin\theta \tag{2.6}$$

in the direction normal to the incident gamma ray, where p_e represents momentum of the scattered electron and p_γ is the scattered photon's momentum and ϕ and θ are the scattering angles.

Using the relativistic equation

$$E_e \approx m_e c^2 + p_e c \qquad (2.7)$$

and equations 2.4 – 2.6 one can easily solve the equation for the energy of the scattered gamma ray photon as

$$E_\gamma = \frac{E}{1 + \frac{E}{m_e c^2}(1 - \cos\theta)} \qquad (2.8)$$

where $m_e c^2$ is the electron's rest mass energy which is equal to 0.511 MeV/c^2.
At θ = 0º the scattered gamma ray has energy almost equal to that of the incident gamma ray with little energy given to the recoiling electron. At θ = 180º, E_γ is reduced to approximately 0.25 MeV when $E_{\gamma.} >> m_e c^2$, this is the maximum recoil energy for the electron but always less than $E_{\gamma.}$ [Lil01].

The probability that a gamma ray might be Compton scattered at an angle θ can be predicted by the use of the Klein-Nishina formula which shows that forward scattering is favoured at high energies [Kno00]:

$$\frac{d\sigma}{d\Omega} = Z r_0^2 \left[\frac{1}{1+\alpha(1-\cos\theta)}\right]^2 \left[\frac{1+\cos^2\theta}{2}\right] \left[1 + \frac{\alpha^2(1-\cos\theta)^2}{(1+\cos^2\theta)[1+\alpha(1-\cos\theta)]}\right] \qquad (2.9)$$

where $\alpha \equiv h\upsilon / m_0 c^2$ and r_0 is the classical electron radius which is approximately 2.8 x 10^{-25} m.

The angular distribution is shown in figure 2.4 and shows a strong tendency for forward scattering at high values of the gamma-ray energy.

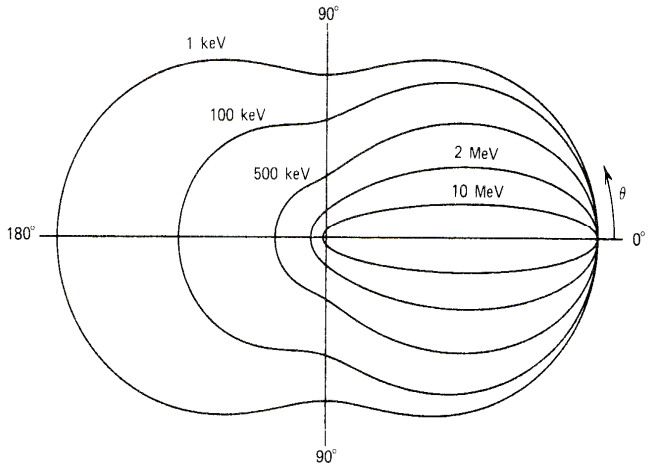

Figure 2.4: A polar plot showing the angular distribution of Compton scattered photons incident from the left into a unit solid angle at the scattering angle θ for the indicated initial energies [Kno00].

2.1.3 Pair Production

A gamma-ray photon can also be absorbed in the nuclear field of an atom, and then two electrons of opposite signs called a negatron(or simple electron) and a positron are emitted. These two leave an atom, each with energy equal to the rest mass of an electron hence the incident photon must have at least 1.02 MeV for this process to take place. Figure 2.5 shows how pair production dominates at high energies compared to the other forms of photon interactions.

The energy of the incident gamma ray is thus represented as

$$h\nu = \left(K_{-} + m_0c^2\right) + \left(K_{+} + m_0c^2\right) \qquad (2.10)$$

where K_- and K_+ are the kinetic energies of the electron and positron respectively. The two kinetic energies are not exactly equal as the positron gets more especially at lower energies [Eva55]. The positron will slow down and eventually annihilate with an electron, resulting in the formation of two gamma rays of energy 0.511 MeV each being emitted in opposite directions for momentum to be conserved [Lil01].

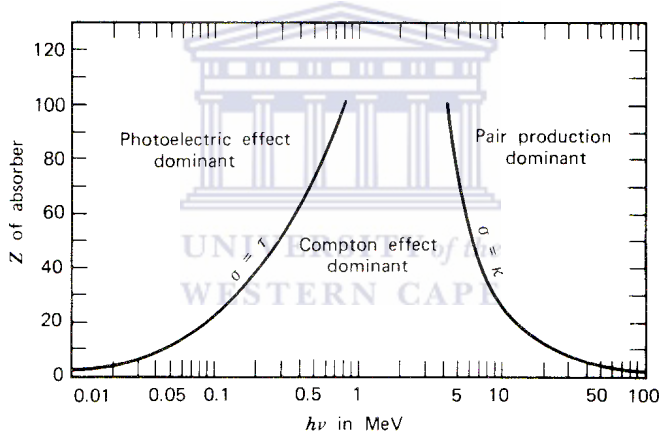

Figure 2.5: Illustration of the three most important types of gamma-ray interaction with lines showing values of Z and hν for which the two neighbouring effects are equal. The linear attenuation coefficients for photoelectric effect, Compton effect and pair production are shown by τ, σ and κ respectively [Kno00].

Other photon processes like Rayleigh scattering where no transfer of energy takes place is ignored for this thesis as the energies where this process is important are less than a few hundred eV for common materials [Kno00].

2.1.4 Attenuation

When gamma rays are travelling through matter they will either be absorbed, scattered or just pass through without interaction. If an absorber material of thickness t is placed between a gamma ray source and the detector, the intensity of the beam of monoenergetic gamma ray photons will decrease as an exponential function of the absorber thickness [Lap72].

The number of transmitted photons I after the introduction of the absorber is given by

$$I = I_0 e^{-\mu_l t} \tag{2.11}$$

where I_0 is the number of transmitted photons without the absorber and μ_l is the linear attenuation coefficient.

The average distance that a gamma ray photon travels before interaction is also important in describing the beam penetration. This is known as the mean free path and it is given by $1/\mu_l$.

At different densities of the same absorber material the values of μ_l will differ and hence the mass attenuation coefficient μ_m is introduced as

$$\mu_m = \frac{\mu_l}{\rho} \tag{2.12}$$

where ρ is the density of the material.

The total mass attenuation coefficient is represented as the sum of the three probabilities of interaction:

$$\mu_m = \mu_{pe} + \mu_{cs} + \mu_{pp} \tag{2.13}$$

where $\mu_{pe,}$ μ_{cs} and μ_{pp} are mass attenuation coefficients for photoelectric effect, Compton scattering and pair production respectively.

2.2 Radioactive decay

Radioactive decay occurs when an unstable nucleus tries to reach stability by releasing particles to the surrounding environment. The nucleus decays predominantly by Alpha (α) decay, Beta (β) decay, Electron capture (EC) and spontaneous fission. The nuclear decay is characterized by the release of energy. The energy released is as a result of mass difference between the parents and daughters after the decay. The total mass of the daughters is always less than the mass of parents.

During α decay an unstable nucleus releases a He nucleus to try and reach stability. This decay is usually characteristic of nuclei with high atomic numbers Z > 83. This type of decay can be represented as

$$ {}^{A}_{Z}X = {}^{A-4}_{Z-2}Y + {}^{4}_{2}He + Q \qquad (2.14) $$

where Q is the surplus energy from the binding energy of the parent nucleus.

The nucleus can also reach stability by either β^- or β^+ decays. In β^- decay a neutron rich nucleus converts a neutron to a proton and releases an electron to reach stability as shown below;

$$ {}^{A}_{Z}X = {}^{A}_{Z+1}Y + \beta^- + \bar{\upsilon} \qquad (2.15) $$

where $\bar{\upsilon}$ is an antineutrino; an almost massless particle which is important in energy and momentum conservation.

In β^+ decay a proton rich nucleus converts a proton to a neutron and releases a positron as shown below;

$$ {}^{A}_{Z}X = {}^{A}_{Z-1}Y + \beta^+ + \upsilon \qquad (2.16) $$

where υ is a neutrino which plays a similar role to the antineutrino. The positron can later annihilate as discussed in the previous section. Most β emitters are not pure β emitters and β emissions are mostly accompanied by gamma radiation.

Another way of nuclear decay is by electron capture. This takes place when a proton captures an electron from an orbital close to the nucleus; therefore EC can take place at energies less than 1.02 MeV. This process is usually accompanied by the releases of an X-ray or Auger electron.

Spontaneous fission is also another decay method where a nucleus splits into two and releases a neutron in the process. There is an enormous amount of energy released by this process on the order of 200 MeV. The products are usually unstable and decay by mostly β^- decay with accompanying gamma decay. This process is not important in this study as the energies involved are too large. Other decay processes are irrelevant for this work but can be found in other texts [Gil95].

Gamma (γ) emission is usually associated with the above decay modes although it is not a change off the nucleus but merely a form of de-excitation by the nucleus from an excited state so as to be more stable. What makes gammas so important is the fact that they are mono-energetic rays similar to alpha particles but unlike betas whose energy is taken away by the neutrino or antineutrino in varying proportions. Gammas are more penetrating than alphas and because of this they are favoured in terms of nuclear energy detection.

2.3 Decay rates and decay series

When a sample of radioactive material decays, the number of radionuclei (N) present at any time t decays at a rate;

$$A = -\frac{dN}{dt} = \lambda N \qquad (2.17)$$

where A is termed the activity and is expressed in Becquerel (Bq) meaning one decaying nucleus per second and λ is the decay constant. The decay constant is the reciprocal of the lifetime τ which is the average time it takes for a nuclide to decay.

The most commonly used time is the half life $t_{1/2}$ which is the time it takes for a number of radionuclides to decay to half its original number. It is related to λ by

$$t_{1/2} = \frac{\ln 2}{\lambda}. \qquad (2.18)$$

The solution to equation (2.17) gives the commonly used radioactive decay law;

$$N = N_0 e^{-\lambda t} \qquad (2.19)$$

with N_0 being the number of radioactive nuclei at t=0.

It is common that a radioactive parent nucleus produces a radioactive daughter nucleus and so on; this is called a radioactive decay chain or series. The daughter nucleus can also decay to granddaughter and so forth [Kra88]. The number of parent nuclei decreases with time according to equation (2.17) which can be arranged as

$$dN_1 = -\lambda_1 N_1 dt \qquad (2.20)$$

whilst the number of daughter nuclei increases as a result of decays of parents and decreases as a result of their own decay as

$$dN_2 = \lambda_1 N_1 dt - \lambda_2 N_2 dt \qquad (2.21)$$

Equation (2.20) can be generalized for any number of generations and the solution to the equation can be found from the Bateman equations [Kra88].

2.4 Environmental Radioactivity

During the creation of the earth many radioactive materials were formed. Many of these have decayed away while some are still decaying as they have half lives which are comparable or longer than the age of the earth [Lil01]. The radioactive nuclides in the environment are known to be either cosmogenic, primordial or of anthropogenic origin.

Cosmogenic radionuclides originate from the cosmic rays from the outer space. Cosmic rays can be of galactic or solar origin and consist mostly of heavy charged particles and ions [Kno00]. These heavy charged particles and ions then interact with the upper atmosphere and produces radionuclides like ^{14}C and ^{7}Be. Other secondary particles like μ and Π mesons, neutrons, electrons and positrons are also produced.

Primordial radionuclides are mostly nuclides from the formation of the earth. Their half lives are mostly comparable to the age of the earth. They are natural radionuclides from the rocks of the earth crust, e.g. ^{235}U, ^{238}U, ^{232}Th, ^{40}K, ^{87}Rb, ^{147}Sm and their radioactive decay products.

Anthropogenic radionuclides are those that man made. These are usually made in the manufacturing of radionuclides like ^{22}Na, ^{137}Cs, ^{131}I and others. They can also leak to the environment around nuclear power stations and nuclear weapon facilities.

In this thesis the focus is on primordial radionuclides although some anthropogenic radionuclides can also be present in soil measurements depending on the place in which the sample was taken.

2.5 Overview of primordial radionuclides

From the list of primordial or terrestrial radionuclides ^{238}U, ^{232}Th and ^{40}K are the only three that can be measured with relative ease because of their abundance and gamma production. Except for ^{40}K these radionuclides decay in a chain with many daughters being formed after a series of α, β and ɣ decay.

2.51 ^{40}K energy line

^{40}K makes up 0.012 % of natural K and it is present in wood, building materials, soil, food we eat and in our bodies. It decays in two modes; one by β^- decay to a stable ^{40}Ca and the other by electron capture to an excited ^{40}Ar state where it de-excites by emitting a ɣ of energy 1.461 MeV as shown in the figure 2.6.

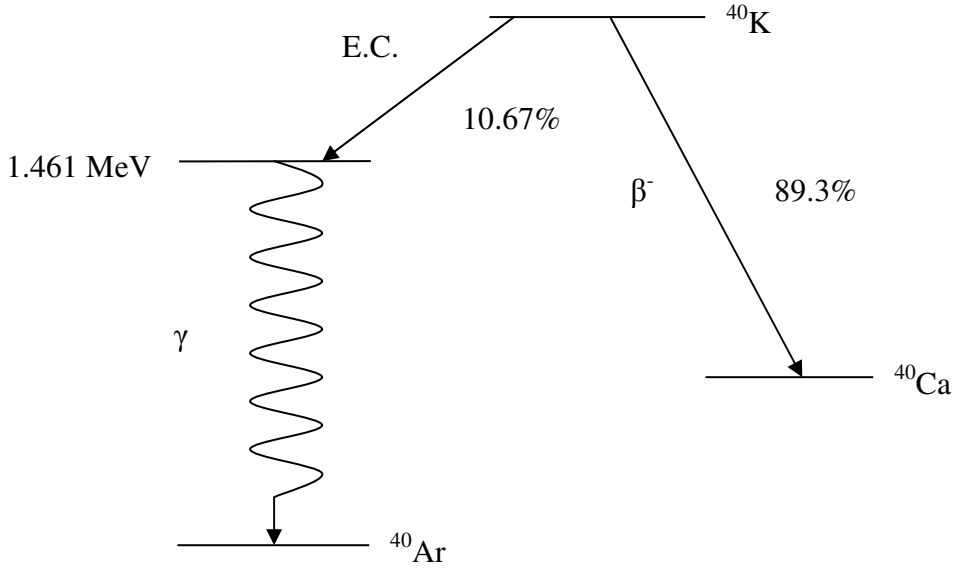

Figure 2.6: Schematic illustration of the decay scheme of ^{40}K.

2.5.2 ^{238}U series

Natural uranium consists of a large amount of ^{238}U (99.25%), a smaller amount of ^{235}U (0.72%) and an even smaller amount of ^{234}U (0.03%). Looking at the decay series of ^{238}U, it α decays to ^{234}Th which β decays to ^{234}Pa and so forth until it decays to ^{206}Pb where it reaches stability as shown in figure 2.7. If the ^{238}U source decays this way undisturbed (no daughter nuclide is removed) then all its daughters are in secular equilibrium with it according to equation (2.21) and so the activity of any of the daughter nuclides equals that of the parent nuclide. The ^{238}U series can be prone to disequilibrium as it contains ^{222}Rn, a noble gas which can easily escape from the sample, therefore samples should be properly sealed for measurements and a waiting period of 10 ^{222}Rn half lives to make sure of equilibrium is needed. There is also a strong possibility of dis-equilibrium resulting from the different chemical behaviour of elements in the decay series. This is of course a lot more difficult for in situ measurements where there is no sealing of samples. ^{226}Ra emits a γ of energy 185.99 keV which makes it difficult to resolve from the 185.72 keV line emitted by ^{235}U, which is one of the reasons ^{235}U is not commonly used for γ spectroscopy.

2.53 ^{232}Th series

Natural thorium consist of 100% ^{232}Th. ^{232}Th α decays to ^{228}Ra then β decays to ^{228}Ac and so forth until it reaches stability in the form of ^{208}Pb as shown in figure 10. The decay series of ^{228}Th contains ^{220}Rn, a gas which can also escape the sample but because ^{220}Rn has a short $t_{1/2}$ (55.8s) equilibrium is quickly re-established. ^{228}Ac, ^{212}Pb, ^{212}Bi and ^{208}Tl are the most significant nuclides for gamma spectrometrists for this decay series.

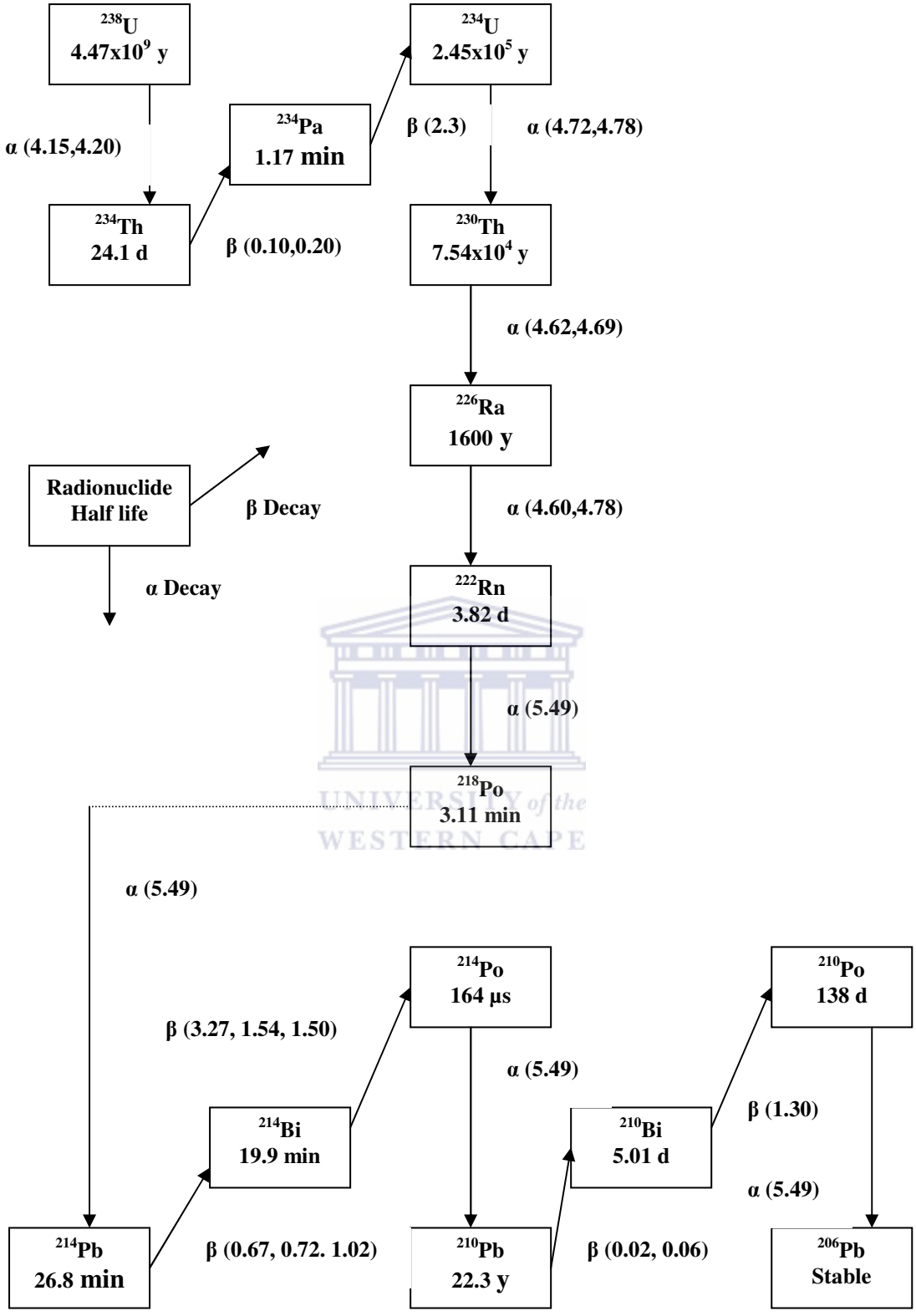

Figure 2.7: Graphical representation of the ^{238}U decay series with ^{226}Ra, ^{214}Pb and ^{214}Bi being the main γ emitting radionuclides. Half lives are indicated inside each block and the branching ratios of each decay mode are also shown in brackets next to the type of decay (Adapted from [Spe04]).

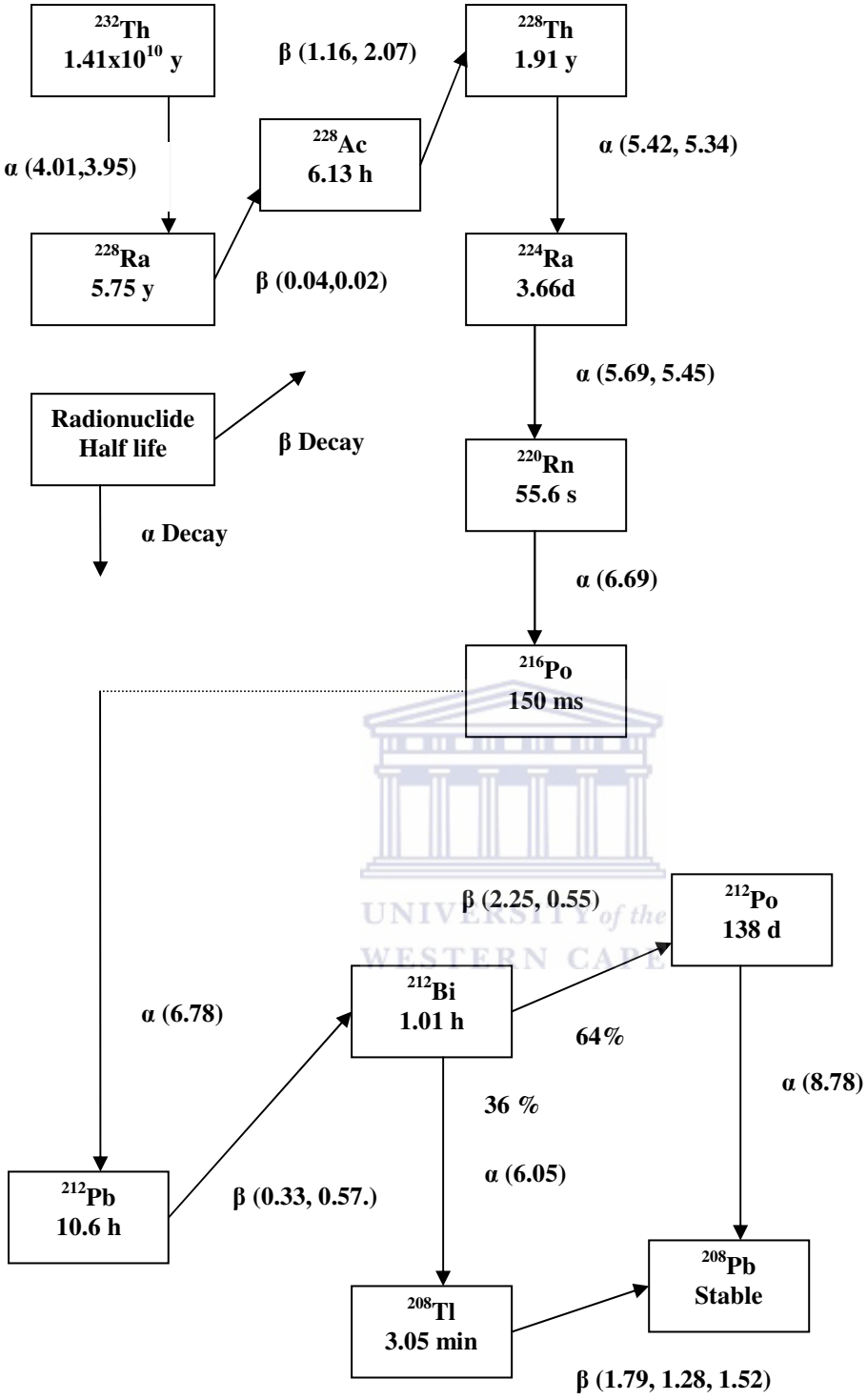

Figure 2.8: Graphical representation of the ^{232}Th decay series with ^{228}Ac, ^{212}Pb, and ^{208}Tl being the γ emitting radionuclides. Half lives are indicated inside each block and the branching ratios of each decay mode are also shown in brackets next to the type of decay (Adapted from [Spe04]).

2.6 Gamma-ray detection

Gamma-ray detectors have been widely used in the detection of natural radiation and applications because of their distinct energy properties and their penetration depth compared to other types of radiation. The three fundamental types of gamma detectors are the semiconductor detectors, organic scintillators and inorganic scintillators.

Semiconductor detectors are formed from semiconductors as the name suggests. They have the best resolution of all available detectors. They have moderate density and Z values e.g. ρ= 5.3 g/cm^3 and Z = 32 for the Ge content in High-Purity Germanium (HPGe) detectors. They have low light output and hence they are usually used for ex-situ measurements. They also have to be cooled with liquid nitrogen to about 77 K to reduce electronic noise [Lil01].

Inorganic scintillators are mostly formed from crystals of alkali metals and halides. Fluorescence depends on the energy level structure of the material's crystal lattice. They have moderate to high density (ρ_{NaI}=3.7g/cm^3, ρ_{BGO}=7.13g/cm^3) and Z (Z_I = 58, Z_{Bi}= 83) values hence high efficiency [Kno00]. They can be operated at room temperature and have a relatively good resolution. The most commonly used are NaI, CsI, BGO and now gaining popularity because of a combination of higher efficiency and better resolution than are the Lanthanum halides [Gil95].

Organic scintillators are mostly formed from aromatic hydrocarbons, they can be crystalline in structure, liquids or plastics. Fluorescence takes place as a result of transitions in the energy level structure of a single molecule. The advantages of using these types of detectors include an option of being moulded to different shapes and sizes and the fast time response they offer especially when loaded with impurities like Tin. They have a disadvantage of poor resolution though, and can also suffer from quenching effects especially liquids when they react with oxygen [Kno00]. Some commonly used organic scintillators are anthracene ($C_{14}H_{10}$) and naphthalene ($C_{10}H_8$).

2.6.1 Scintillation process

The process of scintillation can be simplified as the absorption energy from a gamma-ray by the scintillating material and reemitting that energy as many photons of near optical wavelength. This process is possible because of ionization that takes place when the gamma-ray interacts with the scintillating material. The primary electrons created by the processes outlined in section 2.1 raise secondary electrons to the conduction band leaving holes in the valence band. De-excitation of these raised electrons is usually accompanied by an emission of light photons which are then converted by the electronic part of the detector to an electric pulse using the photo-electric effect. Other crystals like NaI have large band gaps (gap between valence and conduction band) and they need activators like Thallium (Tl) to emit efficient fluorescence [Gil95].

2.6.2 Detector efficiency

The detector efficiency is one of the most important aspects that a gamma spectrometrist looks for in a detector. The high efficient detectors will give you more counts per second and therefore they are the preferred choice for samples with low activity. The efficiency of a detector can be defined in two ways: Absolute or intrinsic. The absolute efficiency can be defined as

$$\varepsilon_{abs} = \frac{\text{no. of pulses recorded}}{\text{no. of radiation quanta emitted by source}} \qquad (2.22)$$

and it is dependent on the detector properties and also on the distance from the source of radiation to the detector.

The intrinsic efficiency can be defined as

$$\varepsilon_{int} = \frac{\text{no. of pulses recorded}}{\text{no. of radiation quanta incident on the detector}} \qquad (2.23)$$

and it is only depended on the type and energy of the incident radiation and also on the detector material [Kno00], [Leo87].

The two efficiencies are related for isotropic sources by a simple equation:

$$\varepsilon_{\text{int}} = \varepsilon_{abs} \times \left(\frac{4\pi}{\Omega} \right) \qquad (2.24)$$

where Ω is the solid angle of the detector from the source position's view [Kno00].

2.6.3 Detector response

When gamma-rays interact with the detectors in the three processes that have been described in section 2.1, a spectrum is observed. This spectrum is called the response function of the detector. Ideally for fixed incident energy the output signal has single fixed amplitude which is a Dirac delta function [Leo87]. Factors such as different interactions inside the detector, detector design and geometry influence the response function.

For a simple case of a gamma ray depositing all its energy to a detector by the photo-electric effect, a full energy peak will form in the spectrum with the value of its energy corresponding to the gamma ray's initial energy. Complications arise in the other two forms of gamma interactions.

In the case of Compton scattering only the energy deposited to the electron is detected, the rest of the energy often escapes with the scattered photon and hence the spectrum will not record a full energy peak but a continuum from zero energy up to the Compton edge as shown in figure 2.9 [Gil95]. Sometimes more than one Compton event may take place and this leads to some events which appear between the Compton edge and the full energy peak. The scattered photon may also be absorbed in the detector before it can escape, which leads to a full energy peak being registered as it happens in faster time (~ ns) than the time resolution of the detector (~ μs).

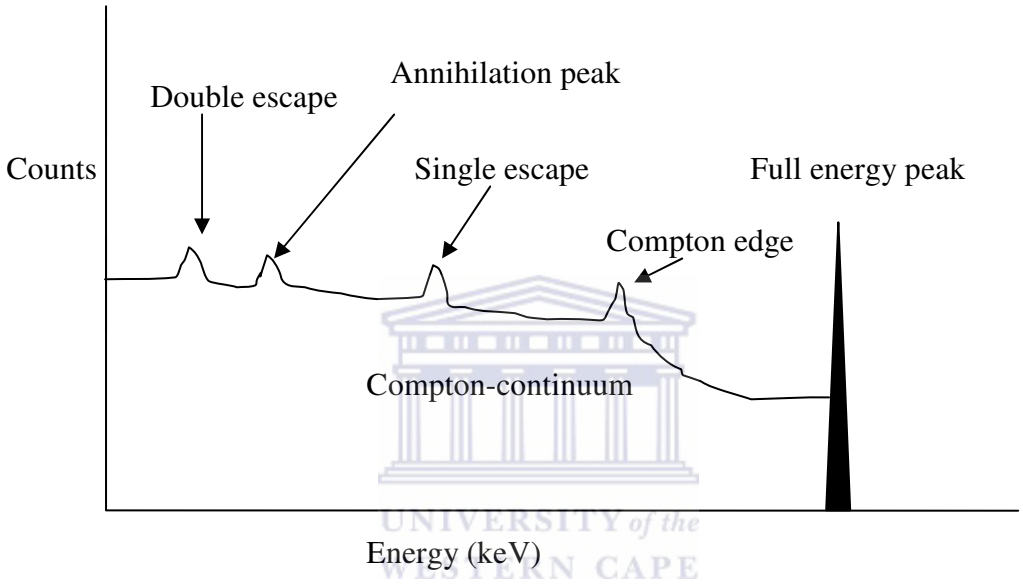

Figure 2.9: A typical example of a spectrum showing different peaks that can be witnessed in a typical detector when photon energies are favourable for all interactions.

If the incident gamma-ray energy exceeds 1022 keV there is a possibility that pair production may take place. If one of the annihilation photons escapes after positron annihilation then a single escape peak may be formed at exactly 511 keV below the full energy peak. If both photons escape then a double escape peak may be formed at exactly 1022 keV below the full energy peak [Gil95]. Similar to Compton scattering the photons may not escape and may be added to form a full energy peak.

Chapter 3 Experimental and Analysis Methods

When measuring natural radiation in soil it is essential to have the right system in place as these measurements constitute very low readings which need an optimized setup. The detector setup and its components are discussed in this chapter (3.1). Thereafter the sample collection, preparation and measurement is explained together with the reference sources used (3.2). Finally a method to extract activity concentration is explained in our analysis method discussion (3.3).

3.1 The NaI (Tl) detector setup.

The NaI detector that was used in this study is situated inside room 147b in the physics department building at UWC. The detector was deliberately placed there and not in the nuclear physics lab to avoid some background counts from radioactive sources in the lab. The setup consists of a NaI detector (with an attached MCA) situated inside a lead castle and connected to a laptop as shown in figure 3.1 below.

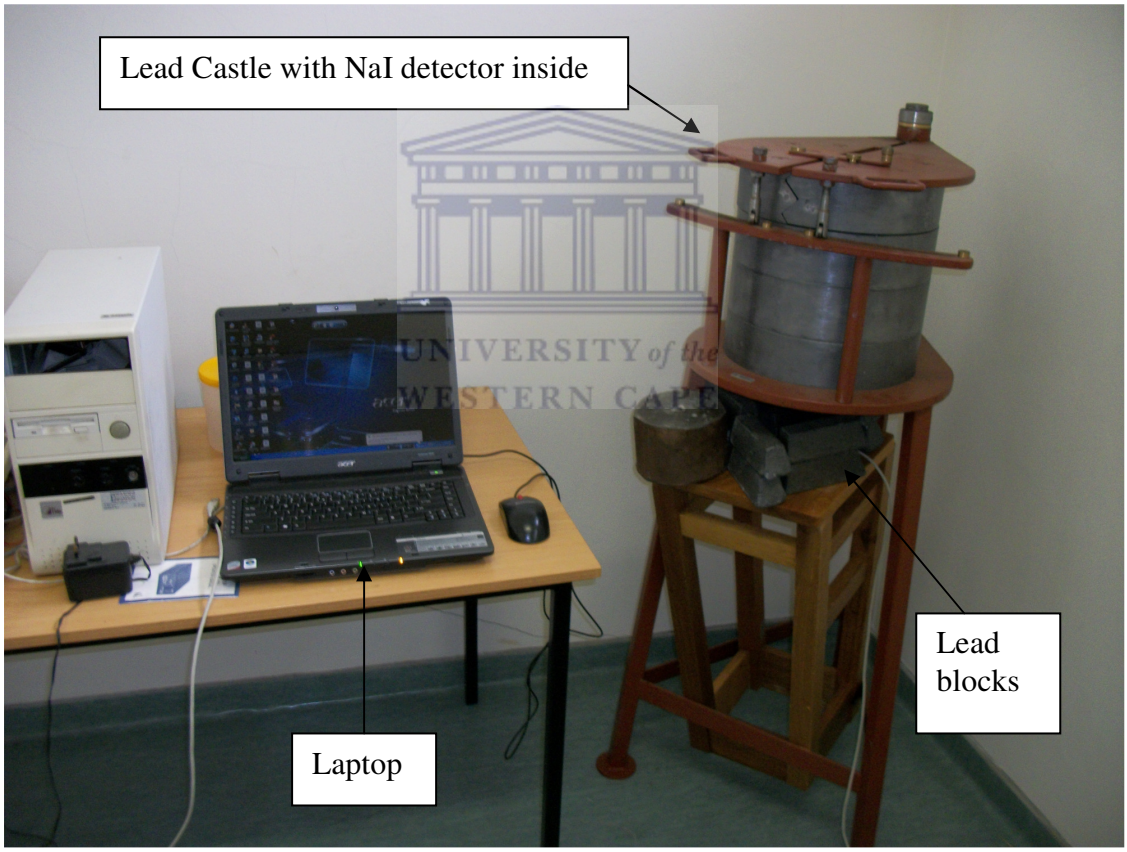

Figure 3.1: A picture of the detection setup that was used showing a lead castle and its stand housing a NaI detector which is then connected to a laptop.

The lead castle which houses the detector and the sample, the NaI detector (with scintiSPEC MCA and USB cable connected to it) and the laptop which has the winTMCA32 scintiSPEC [www03] software for spectrum analysis are the most important components of this setup.

3.1.1 Lead Castle

Natural radioactivity concentrations in soil can be found to be very low, hence background radiation (which comes from U, Th and K in the building material) will be detected and form part of the spectrum. This is undesirable and may lead to incorrect results. A lead castle is usually used to shield the detector and sample to minimize effects of background radiation. Lead is a suitable material for this job as it has high density and high atomic number to stop most of the background radiation. This particular lead castle was designed in a cylindrical shape with layers of semicircular lead discs of 10cm in thickness forming a cylinder. The top of the castle can be opened as shown in figure 3.2 to insert the detector and the samples. The bottom of the castle has a hole which holds the detector and allows any connection from the base of the detector to the laptop in this case. This hole however has been found to be one of the flaws of this design as it is too big and exposes the detector to some background radiation from the floor and the walls of the room. Lead blocks were then placed below this hole to minimize this background radiation as shown in figure 3.1. Background measurements were taken before and after placement of these lead blocks. These blocks reduced the counts in the Th, K and U peaks in the background spectrum by up to 20% as is shown in table 3.1.

Figure 3.2: A picture showing the Lead Castle opened with a sample inside.

The background spectrum was characterised by two significant peaks; the thorium and potassium peaks as shown in tables 3.1 and 3.2.

Table 3.1: Spectral information of the background measurements without lead blocks at the bottom.

Series	Nuclide	Energy (keV)	Live-time (s)	Count rate (cps)
^{40}K	^{40}K	1461	259826.3	0.42
^{232}Th	^{208}Tl	2614	259826.3	0.07

Table 3.2: Spectral information of the background measurements with lead blocks placed at the bottom

Series	Nuclide	Energy (keV)	Live-time (s)	Count rate (cps)
^{40}K	^{40}K	1461	85285.5	0.34
^{232}Th	^{208}Tl	2614	85825.5	0.05

.

3.1.2. The NaI detector and its specification

The NaI detector which was used in this study is a 3" by 3" (75mm X 75mm) crystal. The crystal is encapsulated by an aluminium casing. This particular detector is designed by REXON Components, Inc. The design is such that the detector has a built in amplifier and uses its software for gain and high voltage settings with a scintiSPEC MCA attached at the back and a single USB cable connecting the MCA to a PC as shown in figure 3.1. The crystal is also connected to a photomultiplier tube which is also enclosed inside the aluminium casing.

A B

Figure 3.3: A side view of the NaI detector with the MCA connected at the back (A) and a rear view showing the connectors to the scintiSPEC MCA and the USB cable (B).

- **Photomultiplier tube (PMT)**

Emitted light by the crystal has to be converted to electrons for an electric signal to be read by the MCA. Light is converted at the window which connects the amplifier to the detector. This window is called the photocathode. The photoelectrons then migrate to the photocathode surface where they escape and are accelerated to the first dynode inside the PMT. Light impinges the photocathode with energy of about 3eV and loses some of it when converted to photoelectrons due to electron collision. The already decreased energy has to overcome the potential barrier which exists at any interface between the material and vacuum. The electrons which reach the first dynode 'multiply' and move to the second dynode and so forth. Materials which have negative electron affinity are usually used in the dynodes to increase secondary electrons. The cascade of electrons is then collected in the anode to produce an electric pulse [Leo87].

- **Multi-Channel Analyzer (MCA)**

After the cascade of electrons has been connected to the anode to produce a pulse, the pulse needs to be sorted out according to pulse height to a particular channel in a multichannel memory. This is done by the MCA (target USB MCA scintiSPEC in this case) which utilises an analog-to-digital converter (ADC) to convert the incoming pulse. The MCA then stores the digitized pulses in a memory channel whose address is proportional to the digitized value corresponding to pulse amplitudes [Leo87].

The winTMCA32 scintiSPEC software was used to display counts of gamma rays recorded for a range of lower to higher energies in the form of an energy spectrum. The software is equipped with a hardware setup option to set the gain and high voltage among other things. The gain was set to 1.5 and high voltage to 1050 Volts for these measurements in order to display all the energy peaks from the natural decay series in 1024 channels.

3.1.3 Energy calibration

When a spectrum of counts with respect to channels of any particular nuclide is acquired by the MCA we need to recognise the correct energy for the particular energy peaks. The winTMCA32 scintiSPEC software has a counts versus channel scale or counts versus energy scale. To determine the correct energy for a particular channel the system has to be energy calibrated with sources of known energy peaks. This can be done directly on the winTMCA32 scintiSPEC software by using the energy calibration method and plotting the counts in the region of interest (ROI) versus the corresponding channels. The software uses the following formula to calibrate between two points.

$$E = a(Ch) + b \tag{1}$$

where E is the energy at a particular channel Ch, a being the slope and b is the offset.

When there are more than two points to consider for energy calibration the software uses a quadratic equation:

$$E = a(Ch)^2 + b(Ch) + c \quad (2)$$

where c now becomes the offset.

3.1.4 Energy Resolution

One of the most important aspects of the detector is its energy resolution as it determines whether the energy peaks can be resolved. NaI detectors have good energy resolution compared to other scintillators but far worse when compared to semiconductors like HPGe. The energy resolution of a detector is usually given as a percentage of a full energy peak's Full Width at Half Maximum (FWHM) over the centroid value of that particular energy peak. The smaller the percentage value the better the resolution. Any energy values separated by a value bigger than or equal to the detector's FWHM should be able to be resolved [Kno00].

A short measurement (5 minutes) was done using a ^{137}Cs source to check the FWHM at the source's energy peak of 661 keV. The value is automatically calculated by the software when a region of interest is put around the highest energy. The FWHM was found to be 7.8 % which is close to the manufacture specification of 7.00 %.

3.2 Sample collection, preparation and measurements

A variety of samples which were collected in different places were used in this study. The purpose of this was to get all three natural radionuclides represented in different ratios. These samples were collected in the years 2004 and 2005 and were kept in the ERL at iThemba Labs. The samples were collected from as far as Kloof mine in Westonaria (South of Johannesburg SA), Simonstown, some beach sand from the east coast and some soil from iThemba labs. Spectral information and other details of these samples are given in Table 1. The samples were carried using plastic bags from these places to the ERL were they were dried in a Labotech oven at temperatures of 105 ºC. The samples are then sieved using a mesh with a diameter of 2 mm to remove stones, lumps and organic materials [Map04]. The samples are put inside a Marinelli beaker and weighted using a digital weighing balance (Satorius, model BP2100S, ±0.01 g precision). The following procedure was followed to weigh the sample: Firstly the empty Marinelli was weighed and recorded followed by its lid and copper lid of about 2 mm in diameter. Secondly the sample is poured into the Marinelli which is sealed with the copper disc and its lid and measured again. The difference between the weight of the Marinelli with sample and without a sample is taken as the sample weight. Then finally the Marinelli is sealed with a silicon sealant to make it air tight [Hla09].

The Marinelli beakers are used because of the improved counting rate they give especially for low level counting [Lav96]. This is because they can be designed to fit the detector and therefore surrounds the detector for an improved detector to source

geometry. The marinelli beaker which was used is a 1 litre polypropylene beaker (model VZ-1525) manufactured by Amersham [Ame00]. The geometry and dimension are shown in figure 3.4 below.

Figure 3.4: Picture of the one litre polypropylene Marinelli beaker (model VZ-1525) used to hold samples for radiometric measurements.

Table 3.3: Details about the different samples that were collected and measured.

Sample ID	Live-time (s)	Mass (kg)	Density (g/cm^3)	Total Counts	Count rate (cps)
Anstip beach sand	67401	1.5287	1.53	1549087	22.98
Simonsig soil #P24	66130	1.4930	1.49	2648757	40.05
Simonsig soil #P25	68115	1.6510	1.65	2099197	30.82
iThemba soil #HS1, S1	69088	1.4529	1.45	15627644	226.20
iThemba soil #HS6, S1	162321	1.3446	1.34	3822341	23.55
Kloof sample 50cm	88004	1.4254	1.42	12064132	137.09
Rawsonville soil #B28	69982	1.1258	1.13	3493088	49.91
Rawsonville soil #B31	62806	1.1994	1.20	3184198	50.70

3.2.1 Reference sources for the lab measurements

Three reference sources were used in this study, each one containing a large quantity of either ^{238}U, ^{232}Th or ^{40}K. These sources serve two important purposes: To energy calibrate the system for the expected radionuclides so as to know where certain energy peaks can be expected. Secondly these sources are used as 'standard spectra' in full spectrum analysis method. Some relevant information about these sources is given in table 3.4 [RL148].

Table 3.4: Details about the reference sources used.

Nuclide	Source Code	Mass (kg)	Volume (ml)	Density (g/cm^3)	Activity Concentration ($Bq.kg^{-1}$)
^{238}U	IAEA(RGU-1)	1.40912	1000	1.41	4940
^{232}Th	IAEA(RGTh-1)	1.36494	1000	1.36	3250
^{40}K	IAEA(RGK-1)	1.29080	1000	1.29	16258

3.3 Field (in-situ) measurements procedure

Field measurements were done on Kloof and Southdeep mine dumps. Measurements were done using the 7.5 cm X 7.5 cm NaI (Tl) detector. This detector was mounted on the front of a 4 X 4 Toyota Hilux vehicle at approximately 50 cm above the ground. A Multi-element Detector for Underwater Sediment Activity (MEDUSA) detector was also mounted next to the NaI (Tl) detector for a parallel experiment [www02]. Five different location or spots on the dump were chosen at random with the help of the Kloof dump map shown in figure 3.5 and a GPS system. The spots were then named according to the date that each one was measured. The measurements were done from the 11th to the 17th October 2010. The Southdeep mine dump did not contain any mine tailings yet, as it was still being prepared to become a mine dump. The spot on the Southdeep mine dump was done on the 17th. Unfortunately the software that was used to acquire the spectrum encountered problems on the 14th and the 15th, hence there are no results for those days. The GPS antenna was mounted directly on the Medusa crystal while the GPS device was kept inside the vehicle. A laptop that was connected to the NaI (Tl) detector was also kept inside the vehicle.
When the detector was connected as shown in figure 3.6, measurements were taken for about an hour (except for the Southdeep stationary point where measurements were done only for 30 minutes because of lack of time). Some details about the count rate of these measurements are given in table 3.5.

Table 3.5: Details about the different locations were stationary measurements were done.

Location	Total Counts	Live time (s)	Count rate (cps)
Kloof 13/10	2289008	2589	884.2
Kloof 16.1/10	1655870	3121	530.6
Kloof 16.2/10	1423109	2230	638.3
Kloof 17/10	1289202	2107	612.0
Southdeep	273939	1673	163.7

Figure 3.5: An aerial view of the Kloof mine dump.

Figure 3.6 The NaI (Tl) detector mounted next to the Medusa detector in front of 4 X 4 vehicle.

The standard spectra for the field measurements were acquired from calibration pads at Lanseria Airport. The pads consist of soil samples containing large quantities of either ^{238}U, ^{232}Th or ^{40}K. More relevant information about the sources is given in table 3.6.

Table 3.6: Activity concentration of the three radionuclides that were used as standard spectra.

Calibration Pads	K_2O	U_3O_8 (ppm)	$Th0_2$ (ppm)
Calibration Pad 1	0.26 ± 0.06	4.3 ± 0.3	158 ± 7
Calibration Pad 2	0.24 ± 0.05	67.0 ± 4.0	7.4 ± 0.1
Calibration Pad 3	6.1 ± 0.2	0.9 ± 0.2	1.9 ± 0.2

3.4 Data Analysis

After the MCA and detector system has measured the gamma energy spectrum, the next critical point is to analyse the spectrum so as to extract the information you need. In this study the interest was to get a close approximation of the activity concentrations of ^{238}U, ^{232}Th and ^{40}K nuclei. The Full Spectrum Analysis (FSA) method was used in this study rather than the frequently used Windows Analysis (WA) method. The WA is described briefly below and the FSA is described in more detail next.

3.4.1 Windows Analysis

The windows analysis method is typically used when using high resolution detectors like Germanium detectors where energy peaks are clearly distinct from one another. This method utilises a Region of Interest (ROI) around a full energy peak and looks at the number of counts in that particular 'window'. The scintiSPEC software uses a peak search option to find the ROI for well defined peaks, or you can manually select the region of interest using the ROI option. The software gives the value of the counts, count rate and FWHM of the particular ROI.

The activity concentration (in Bq/kg) of the gamma energy nuclide of interest is given by

$$A_{Conc} = \frac{C_{Ni}}{ML_t\varepsilon_E r_B} \tag{3.1}$$

where C_{Ni} is the net counts at a particular ROI, M being the mass of sample, L_t the live time (real time it took to measure minus dead time) with r_B and ε_E respectively being the branching ratio and detection efficiency of a particular energy line E.

The 1765 keV (^{214}Bi), 2614 keV (^{208}Tl) and 1416 keV (^{40}K) are often used in activity calculations of ^{238}U, ^{232}Th and ^{40}K respectively [Gil95].

3.3.2 Full Spectrum Analysis (FSA)

The method that was used to calculate the activity concentrations of U, Th and K in this work is the full spectrum analysis method. The FSA method uses three standard spectra which ideally should each contain one of the above mentioned radionuclides. The ideal case is not achievable as the standard spectra will also contain some other trace elements of more than one radionuclide, with one radionuclide being the most dominant by a big margin. A standard spectrum of any radionuclide *X* then represents an expected response of the detector when exposed to an activity concentration of 1Bq/kg of a radionuclide *X* in a specific geometry [Hla05],[New08]. The sum of these three standard spectra X_j multiply by the activity concentration C_j of the individual radionuclides plus a background spectrum *BG* should then equal to the measured spectrum *Y* [Hen03].

The FSA method utilises 'almost' the whole spectrum including the continuum, in contrast to the WA method which only uses the 'window' around the full energy peak. The FSA hence has an advantage over the WA method because of using all the spectral features and thereby reducing the statistical uncertainties in the measurements.

- **Acquiring the standard spectra**

The standard spectra for the samples in table 3.4 were measured using the winTMCA32 scintiSPEC software, where counts versus channel number were acquired. The spectrum was energy calibrated and exported to an Excel spreadsheet. A Microsoft Excel VBA program was written to arrange the data to two columns; one for channels and the other for counts. Another programme was written to re-bin the spectra. The spectra were re-binned such that each channel corresponds to 5 keV. The re-binning exercise was necessary to correct for energy calibration variations between the standard spectra and the measured spectra which are usually witnessed because of gain drifts by mostly temperature variations. A background spectrum was measured using a Marinelli beaker filled with water. The background spectrum was also re-binned and subtracted from the standard spectrum which resulted in the spectra shown in figures 3.7, 3.8 and 3.9. The re-binned background spectrum is shown in figure 3.10.

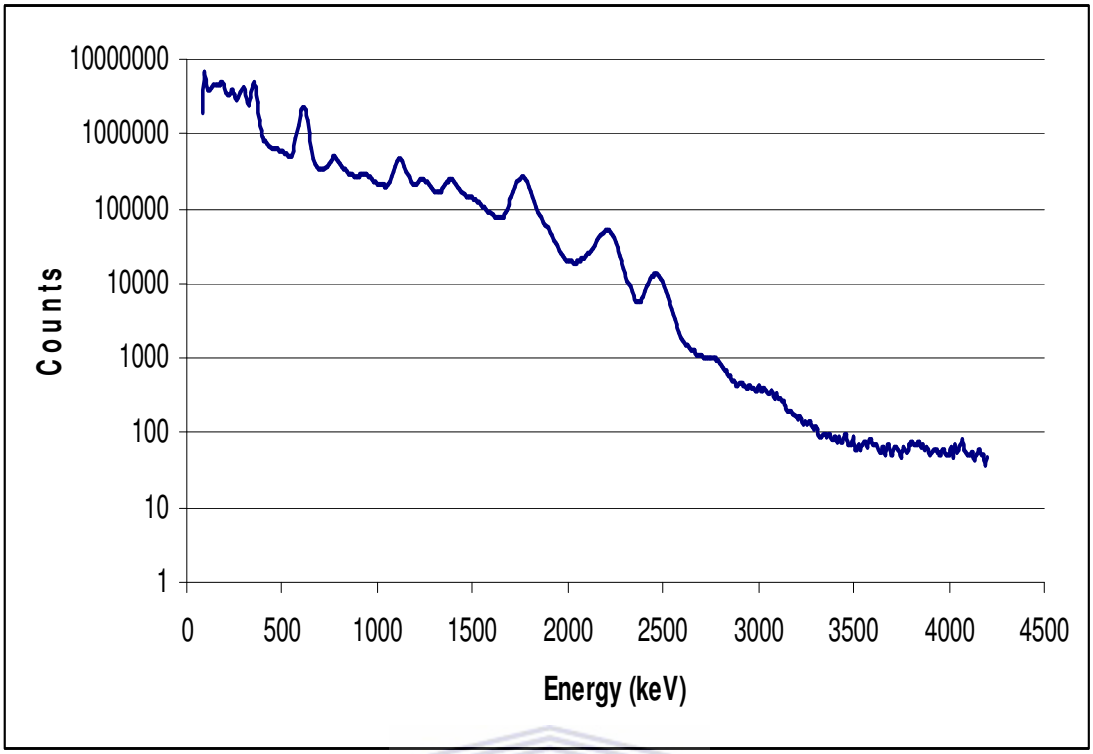

Figure 3.7: Re-binned spectrum of Uranium standard source.

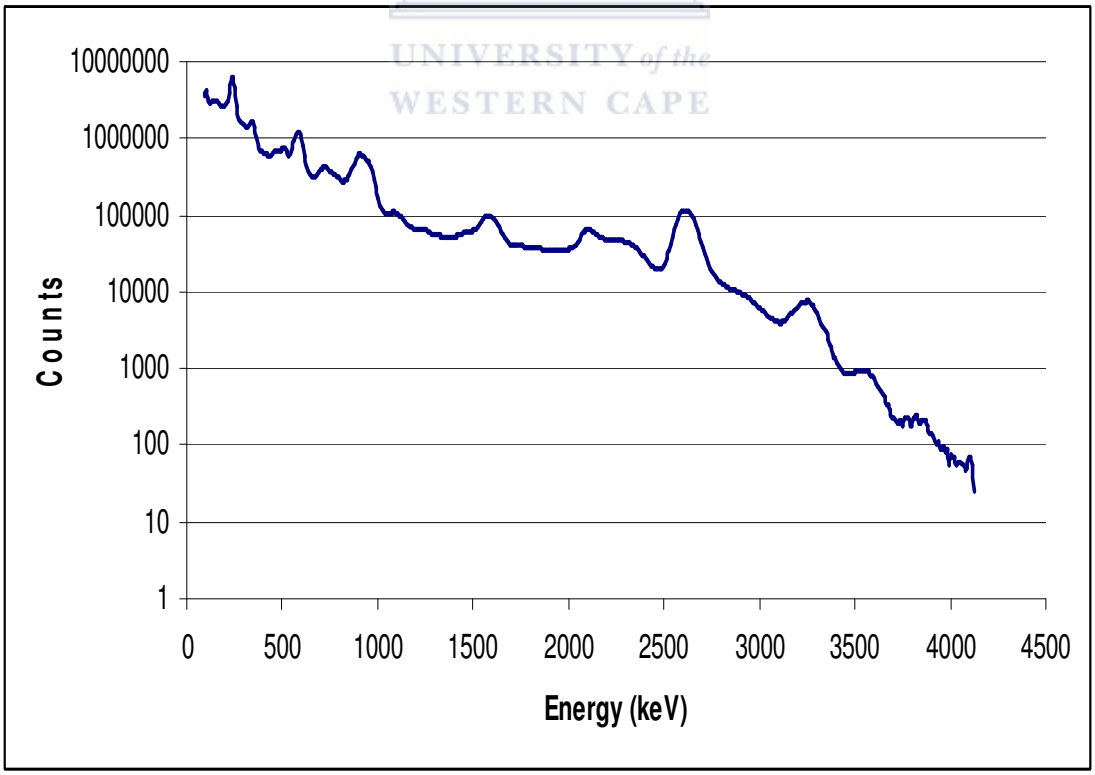

Figure 3.8: Re-binned spectrum of Thorium standard source.

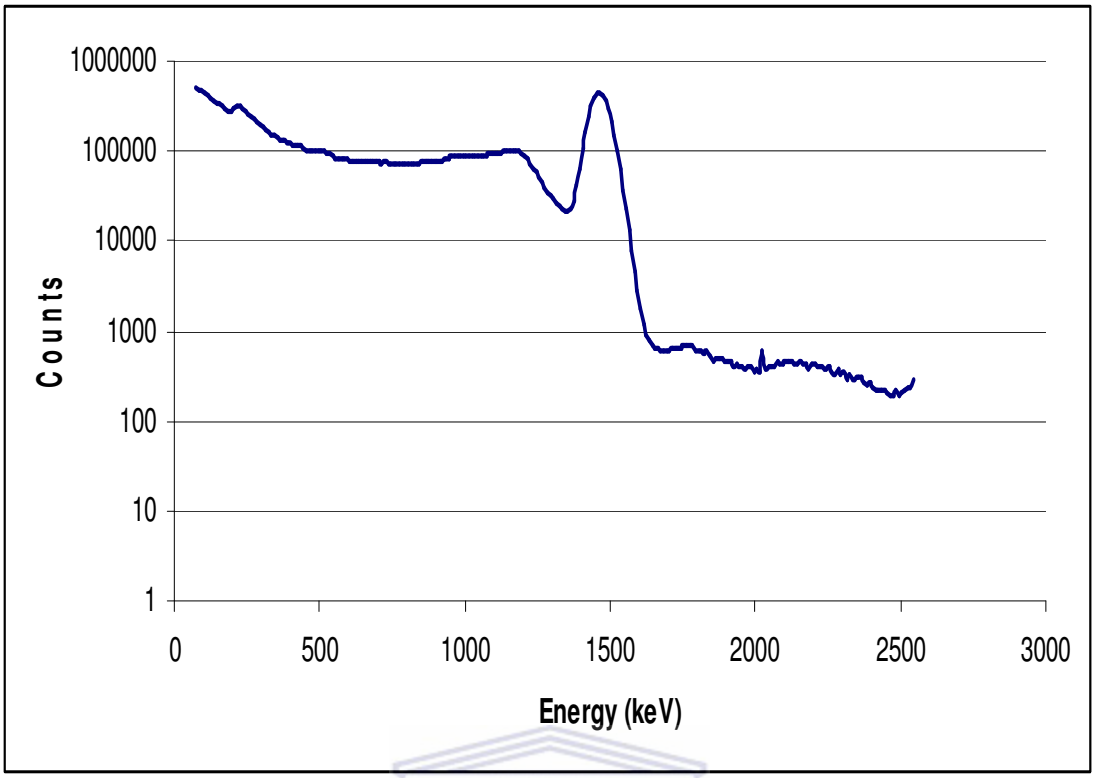

Figure 3.9: Re-binned spectrum of Potassium standard source.

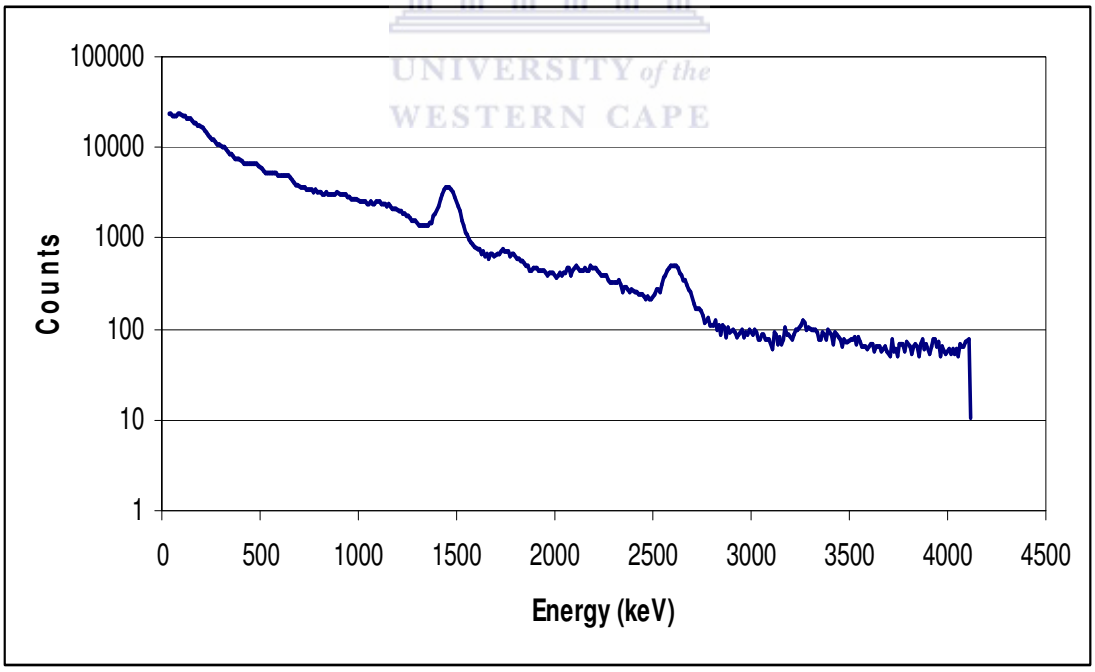

Figure 3.10: Re-binned spectrum of background measurement.

- **Chi-square minimisation procedure**

When all the spectra are re-binned and normalised with respect to live-time, mass and their activity concentrations, the next step is to fit the measured spectrum onto the standard spectra. The activity concentration will therefore be the values of C_j that give the best fit of the measured spectrum Y using to the standard spectra $X_j(i)$. The goodness of the fit is tested by using a least square method to find the optimal activity concentrations. The activity concentrations can then be extracted when the reduced chi-square value:

$$\chi_{red} = \frac{1}{n-m} \sum_{i=lec}^{n=hec} w(i) \left[Y(i) - \sum_j C_j X_j(i) - BG(i) \right]^2 \qquad (3.2)$$

is a minimum. The counts in the measured spectrum, standard spectra and the background spectrum in channel i are represented by $Y(i)$, $X(i)$ and $BG(i)$ respectively. The activity concentration is represented by C_j for different radionuclides j, hence j runs from 1 to 3; *lec* and *hec* represent the lowest and the highest energy cut off respectively; the factor n-m represents the degrees of freedom where n is the number of bins used and m the number of parameters. The weighting factor $w(i)$ is given as the inverse of the sum of the variances of the measured spectrum and the standard spectra weighted by their contributions.

Chapter 4 Results and discussion

In this chapter we first consider the results from an experiment on the spectral drift of this detector and then the activity concentrations of each sample that was measured is presented together with their chi-squared value. The figures showing the measured and the fitted spectra are also presented and the results are then discussed.

4.1 Spectral drift

One of the problems associated with this detector is the instability of the spectrum it produces. Sometimes the spectrum will tend to shift due to factors like temperature changes of the detector or associated electronics and/or counting rate changes [Rob09], [Mos06]. Figure 4.1 shows the shift of the centroid peak of a ^{137}Cs source at 662 keV measured every hour for 48 hours and figure 4.2 shows the room temperature changes at the same time.

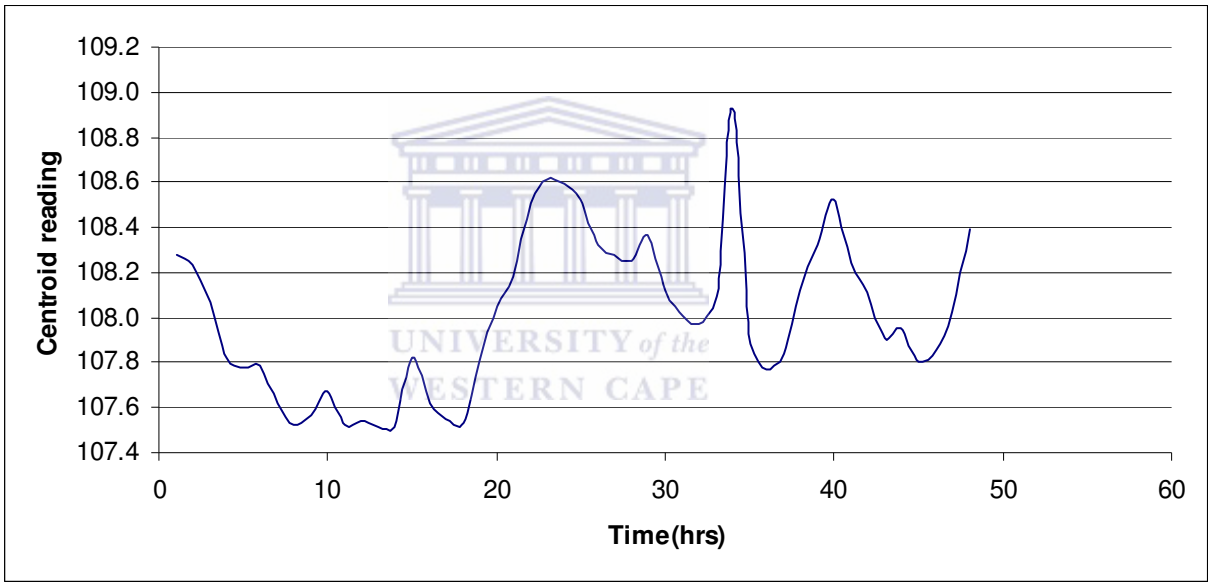

Figure 4.1: A figure showing centroid fluctuations when a ^{137}Cs source was measured using the NaI detector.

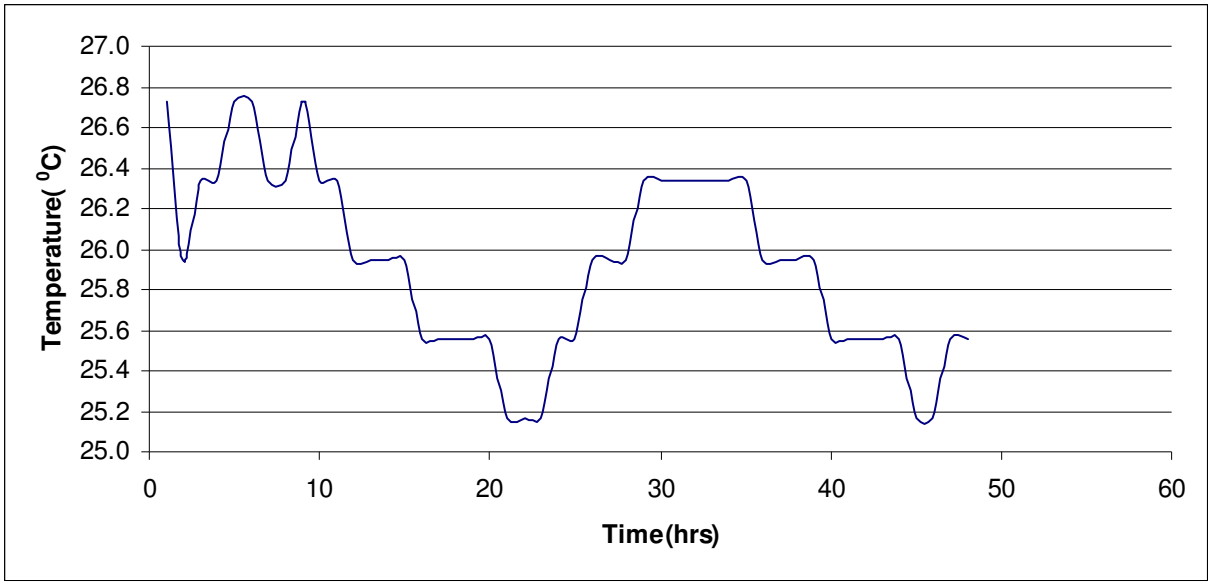

Figure 4.2: A figure showing room temperature fluctuations at the time when the gamma rays from ^{137}Cs was measured using the NaI detector.

4.2 Discussion on the spectral drift results

The results for the centroid shift are presented in figure 4.1. They show a difference of 1.42 channels between the minimum and the maximum. This value translates to 4 keV when taking the calibration equation into account. This is enough to affect the accuracy of your fit or values especially when using full spectrum analysis.

The temperature readings are shown in figure 4.2. The graph shows room temperature readings which do not fluctuate much with a difference of only 1.56 ºC between the minimum and the maximum value.

The first centroid reading was recorded at 11:49 am and its position kept on fluctuating for the rest of the 48 hours as shown in figure 4.1. The room temperature reading was not uniform but it did not change much. The small changes in room temperature do not seem to contribute to the spectral shift as there were some instances when the room temperature did not change but the centroid reading changed noticeably (e.g from 31st hour to 35th). There were also some instances when the room temperature would be higher but the centroid reading lower and vice-versa (e.g 6th and 23rd hour).

The two graphs do not show a correlation or some sort of dependence at all. This shows that room temperature is not a major factor if there is not much difference in temperatures. The drift in the spectrum should therefore be attributed to factors like the temperature fluctuations in the detector electronics itself.

4.3 Sample results

Eight samples were measured using the NaI detector and the fit was done by the least-squared method as described in section 3.3.2. These samples were analysed firstly using Microsoft Excel, where the counts of the standard spectra were fitted to the sample spectrum (also known as the measured spectrum). The best fit was obtained by varying the 3 concentration parameters in equation 3.2 manually to obtain the lowest χ^2 value. In some cases the concentration were adjusted to fit the prominent peaks well as the best fit 'by eye' did not always match the lowest χ^2 value. A detailed discussion of this will follow in section 4.6. Figures 4.3-4.10 show the measured spectra from these samples and also the fitted curve is shown on each figure. The activity concentrations were also calculated using the least squares method in MATLAB [www04]. The MATLAB procedure and results are discussed in sections 4.5 and 4.6. The activity concentration results are summarised in tables 4.1 to 4.2.

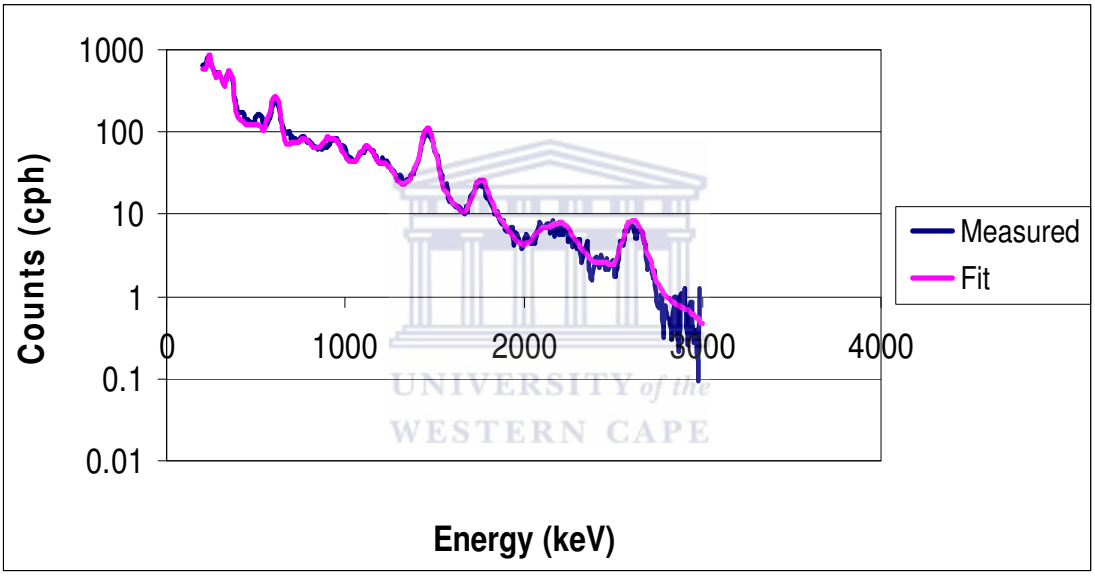

Figure 4.3: A background subtracted spectrum in counts per hour of the Anstip beach sand with the fitted spectrum for energies from 205 keV to 3005 keV.

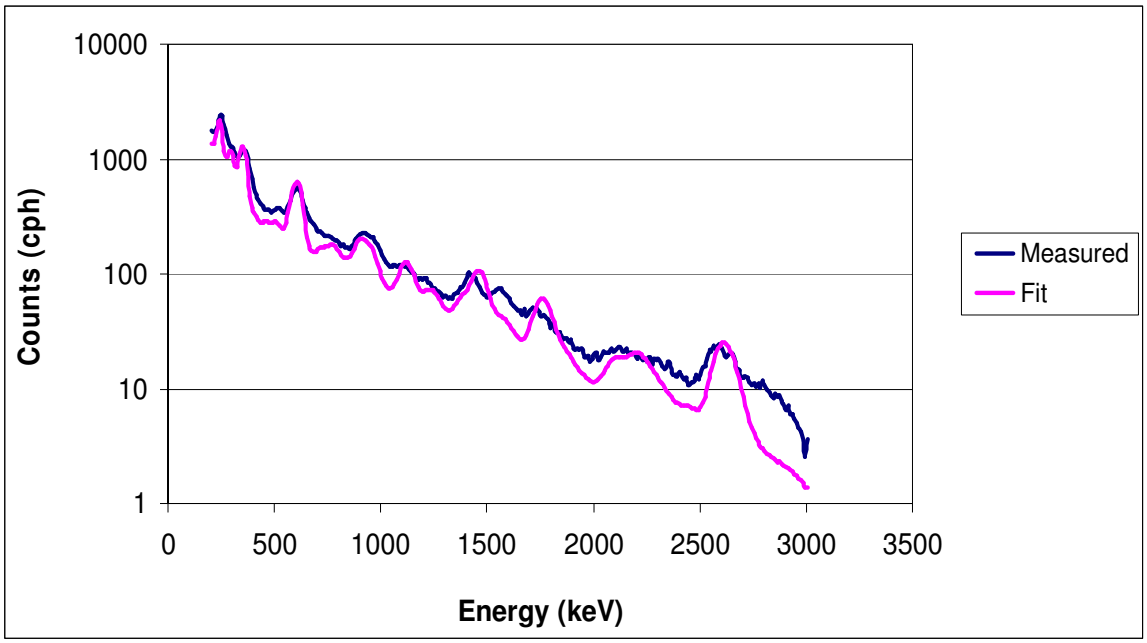

Figure 4.4: A background subtracted spectrum in counts per hour of the Simonsig soil #P24 with the fitted spectrum for energies from 205 keV to 3005 keV.

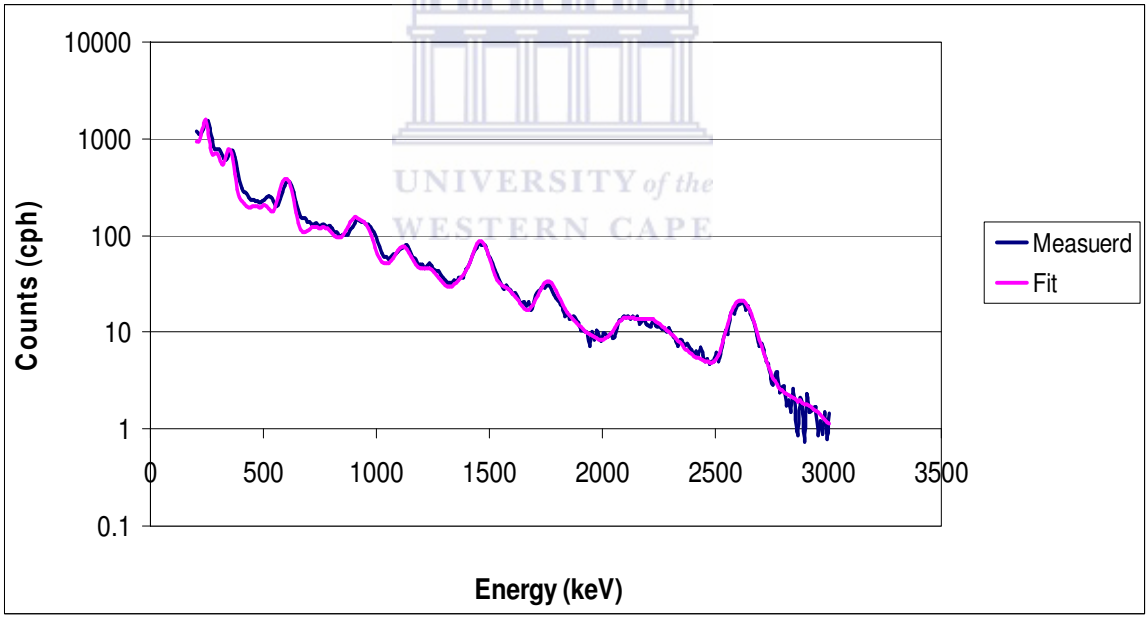

Figure 4.5: A background subtracted spectrum in counts per hour of the Simonsig soil #P25 with the fitted spectrum for energies from 205 keV to 3005 keV.

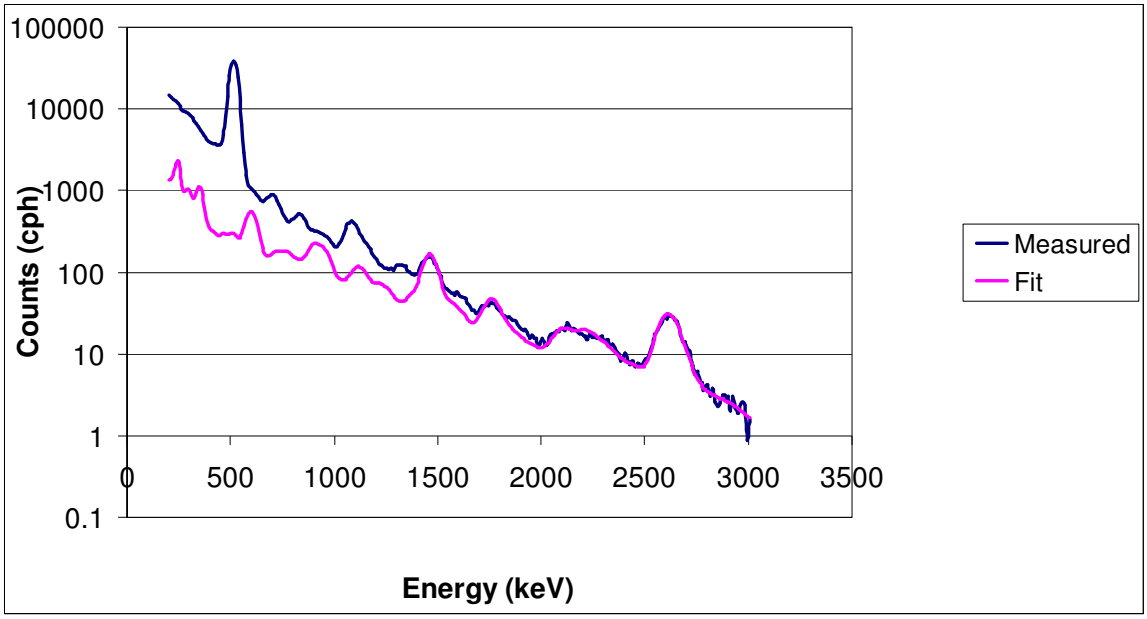

Figure 4.6: A background subtracted spectrum in counts per hour of the iThemba soil HS1 sample with the fitted spectrum for energies from 205 keV to 3005 keV. The poor fit is caused by the presence of anthropogenic radionuclei.

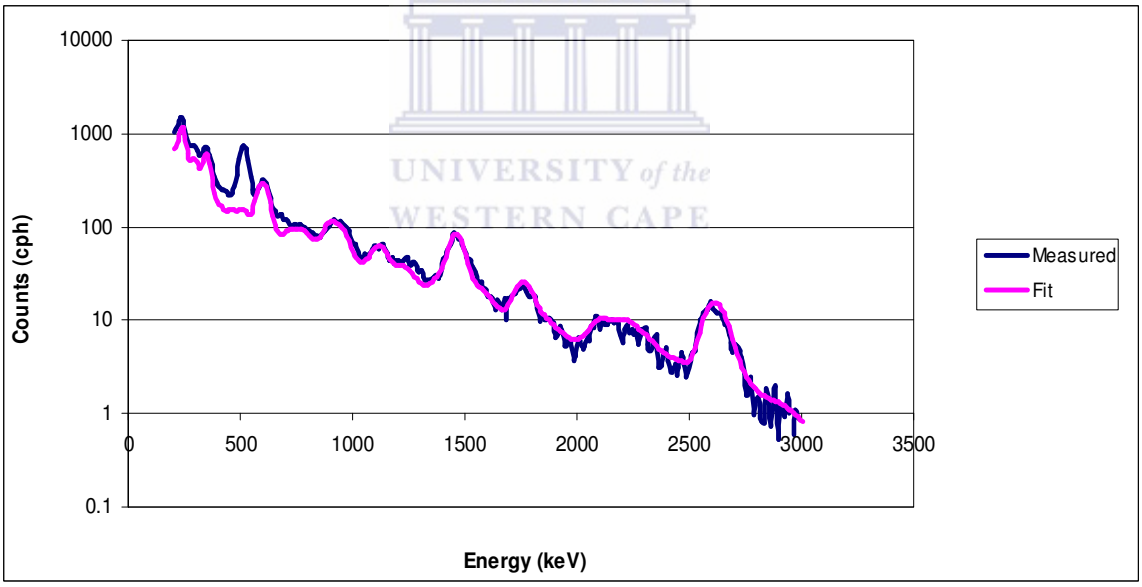

Figure 4.7: A background subtracted spectrum in counts per hour of the iThemba soil HS6 with the fitted spectrum for energies from 205 keV to 3005 keV.

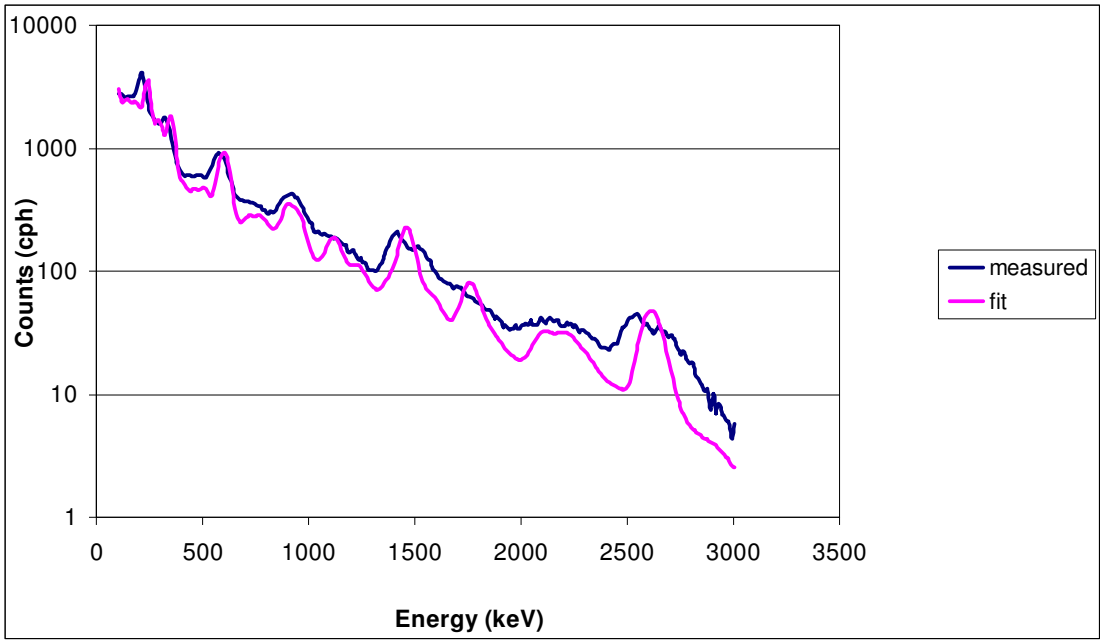

Figure 4.8: A background subtracted spectrum in counts per hour of the Rawsonville soil #B28 with the fitted spectrum for energies from 205 keV to 3005 keV.

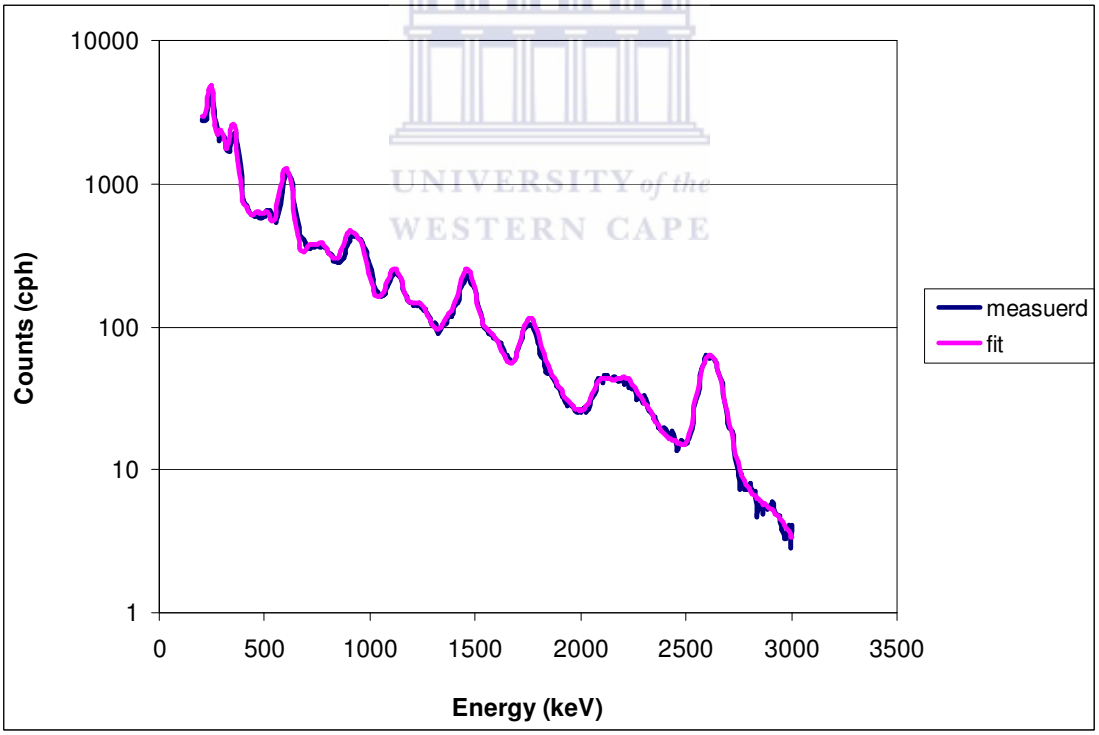

Figure 4.9: A background spectrum in counts per hour of the Rawsonville soil #31 with the fitted spectrum for energies from 205 keV to 3005 keV.

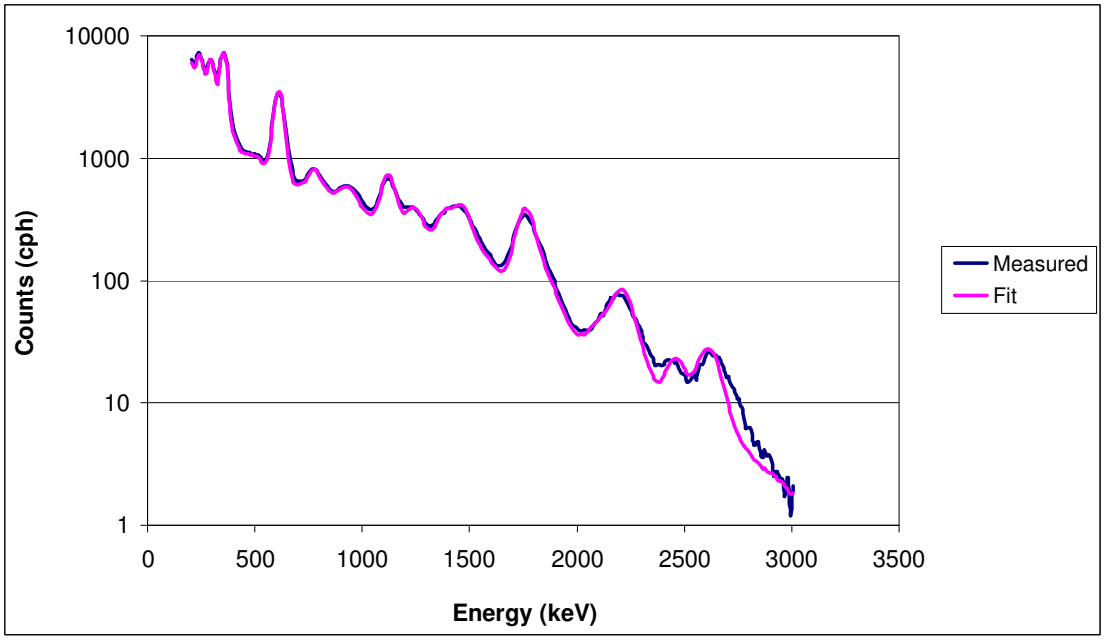

Figure 4.10: A background subtracted spectrum in counts per hour of the Kloof sample with the fitted spectrum for energies from 105 keV to 3005 keV.

Table 4.1: Activity Concentrations for the different samples and their respective chi-squared values calculated using a least-squared method manually in Microsoft Excel.

Sample ID	^{238}U (Bq/kg)	^{232}Th (Bq/kg)	^{40}K (Bq/kg)	χ^2
Anstip beach sand	16 ± 1	7 ± 1	79 ± 6	12
Simonsig soil #P24	36 ± 1	21 ± 1	60 ± 17	159
Simonsig soil #P25	18 ± 1	18 ± 1	57 ± 11	52
iThemba soil #HS1, S1	25 ± 20	26 ± 15	120 ± 400	30450
iThemba soil #HS6, S1	14 ± 1	13 ± 1	60 ± 20	307
Kloof sample 50cm	256 ± 10	22 ± 1	190 ± 20	65
Rawsonville soil #B28	44 ± 8	40 ± 4	153 ± 50	357
Rawsonville soil #B31	64 ± 4	53 ± 3	155 ± 30	104

Table 4.2: Activity Concentrations for the different samples, calculated using a least-squared method using a MATLAB program.

Sample ID	^{238}U (Bq/kg)	^{232}Th (Bq/kg)	^{40}K (Bq/kg)	χ^2
Anstip beach sand	16.7 ± 0.1	6.9 ± 0.1	77 ± 2	9
Simonsig soil #P24	36.5 ± 0.6	28.9 ± 0.4	68 ± 10	100
Simonsig soil #P25	21.6 ± 1.8	18± 2	63 ± 30	45
iThemba soil #HS1, S1	130 ± 30	130 ± 20	-70 ± 490	22496
iThemba soil #HS6, S1	11.9 ± 0.3	12.7 ± 0.2	46 ± 6	119
Kloof sample 50cm	256.7 ± 0.5	28.2 ± 0.3	194 ± 8	46
Rawsonville soil #B28	37.5 ± 1.7	44.9 ± 1.1	230 ± 30	301
Rawsonville soil #B31	65.0 ± 0.8	46.8 ± 0.5	156 ± 13	89

4.4. Field results

The measurements on the Kloof mine dump were done by the method illustrated in section 3.3.2. The measured and the fitted spectra for the five measurements are shown in figures 4.11-4.15 and the activity concentration values are summarised in tables 4.3 and 4.4.

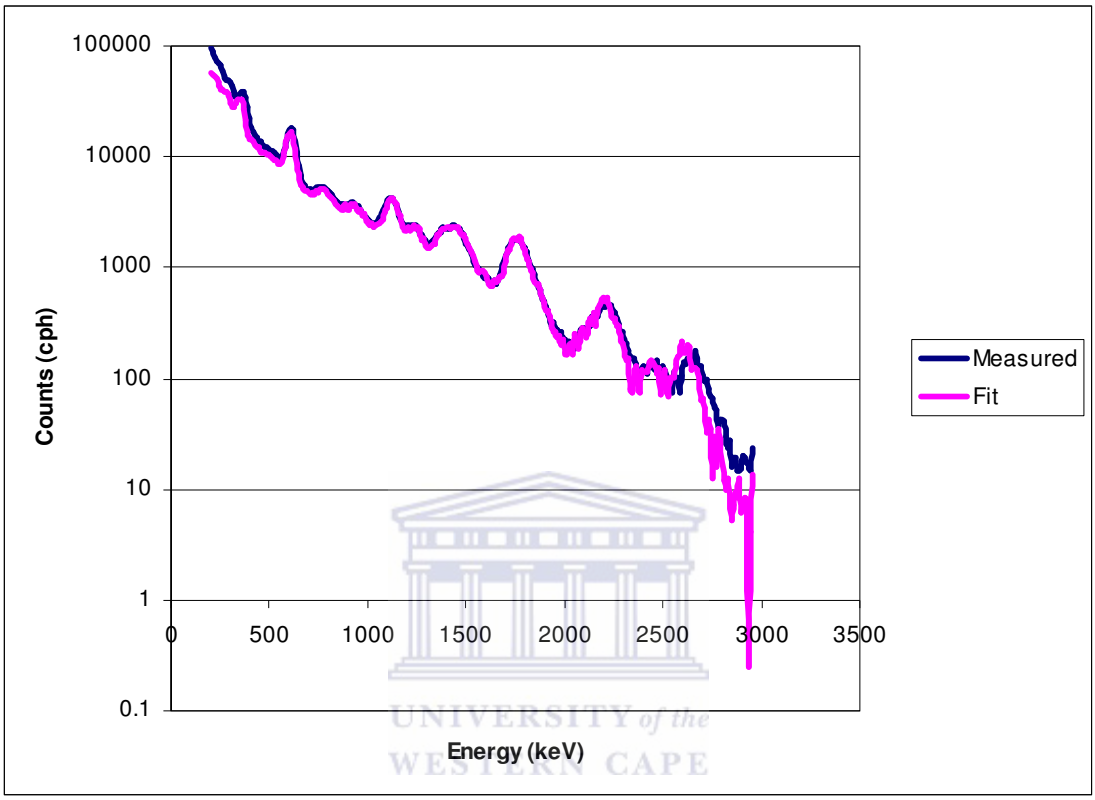

Figure 4.11: A spectrum measured on the stationary point Kloof 13/10 with the fitted spectrum for energies from 205 keV to 3005 keV.

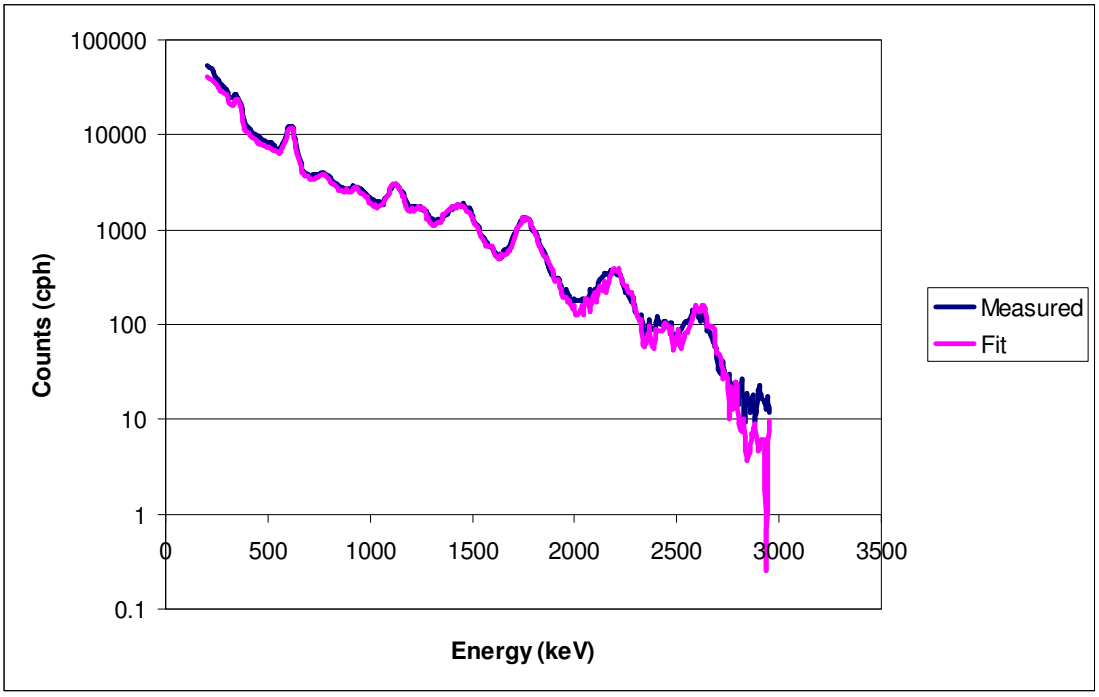

Figure 4.12: A spectrum measured on the stationary point Kloof 16.1/10 with the fitted spectrum for energies from 205 keV to 3005 keV.

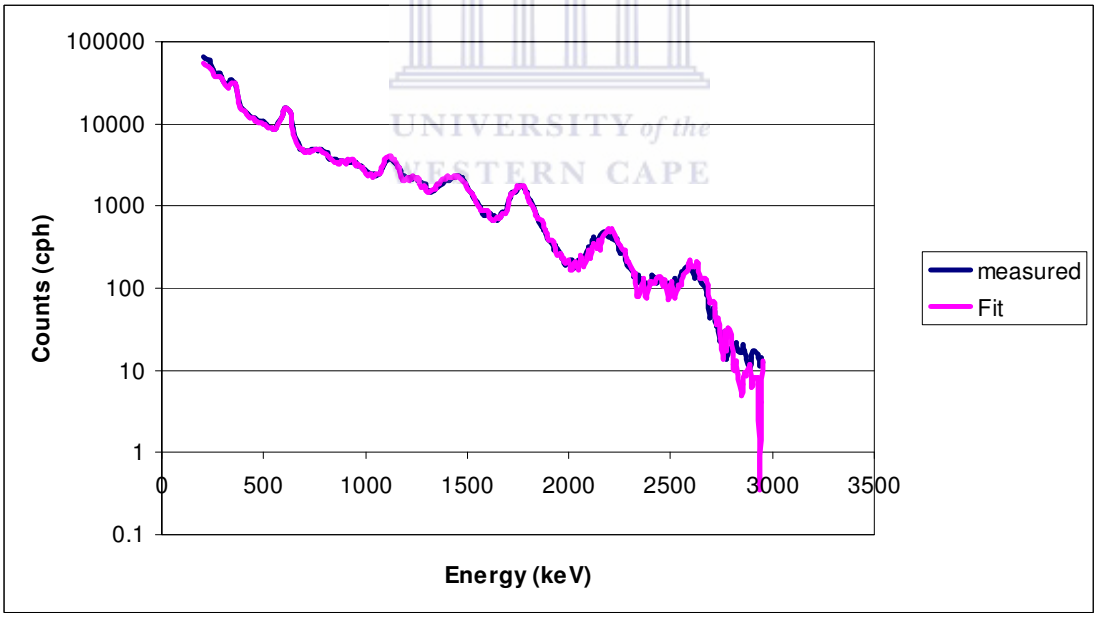

Figure 4.13: A spectrum measured on the stationary point Kloof 16.2/10 with the fitted spectrum for energies from 205 keV to 3005 keV.

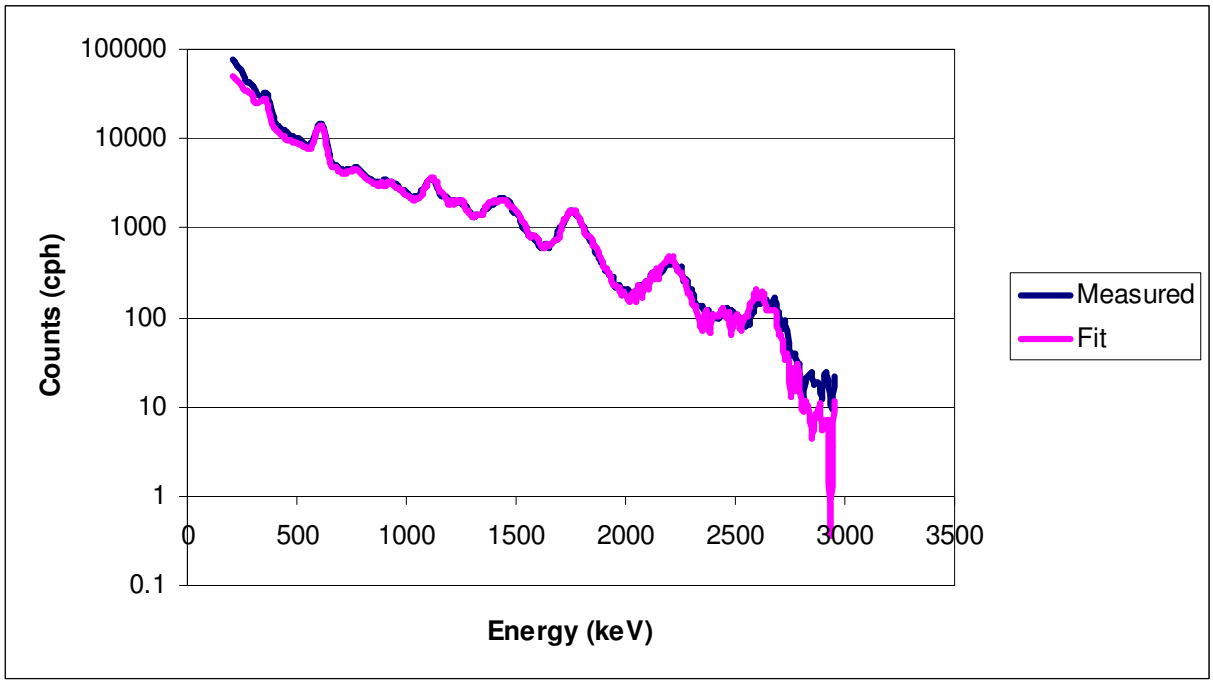

Figure 4.14: A spectrum measured on the stationary point Kloof 17/10 with the fitted spectrum for energies from 205 keV to 3005 keV.

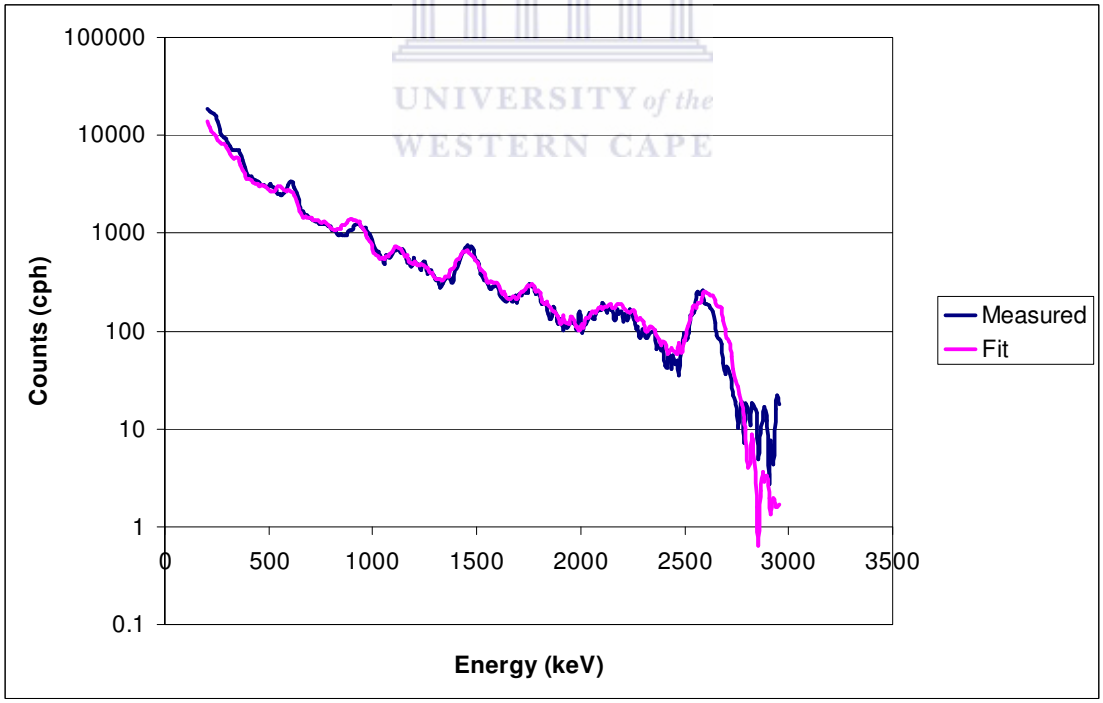

Figure 4.15: A spectrum measured on the stationary point Southdeep with the fitted spectrum for energies from 205 keV to 3005 keV.

Table 4.3: Activity Concentrations for the different samples, calculated using a least-squared method using Microsoft Excel.

Sample ID	^{238}U (Bq/kg)	^{232}Th (Bq/kg)	^{40}K (Bq/kg)
Kloof 13/10	360 ± 4	7 ± 5	250 ± 40
Kloof 16.1/10	260 ± 10	7 ± 17	230 ± 90
Kloof 16.2/10	329 ± 15	11 ± 30	270 ± 180
Kloof 17/10	307 ± 11	10 ± 30	240 ± 170
Southdeep	35 ± 15	46 ± 7	160 ± 60

Table 4.4: Activity Concentrations for the different samples, calculated using a least-squared method using MATLAB.

Sample ID	^{238}U (Bq/kg)	^{232}Th (Bq/kg)	^{40}K (Bq/kg)	χ^2
Kloof 13/10	360 ± 7	23 ± 7	250 ± 80	77
Kloof 16.1/10	254± 3	20 ± 3	250 ± 30	13
Kloof 16.2/10	339 ± 3	18 ± 3	270 ± 30	6
Kloof 17/10	310 ± 5	20 ± 5	230 ± 60	44
Southdeep	31 ± 2	41± 2	150 ± 17	28

4.5 Comparison between the Microsoft Excel and Matlab results

Activity concentration results which were analysed using Microsoft Excel were compared to those ones which were analysed using MATLAB. The MATLAB results were obtained by using *nlinfit,* a function that is available in MATLAB's statistical toolbox. This function was used to automatically estimate the activity concentration that best satisfy equation 3.2 (i.e. the lowest χ^2 value). The *nlinfit* function may be followed by another function *nlparci* which makes use of a covariance matrix to estimate uncertainties for the coefficients (activity concentration values in this case). Figures 4.16 – 4.21 show the comparison between the two. Figures 4.22 to 4.24 also shows three examples of MATLAB plots as compared to the Microsoft Excel plots already shown in section 4.3. The discussion on the comparison of these results follows in section 4.6. Due to high uncertainties in some of the activity concentration the error bars were not included on the bar graph, but can be read from the tables 4.1 – 4.2.

4.5.1 Sample measurements

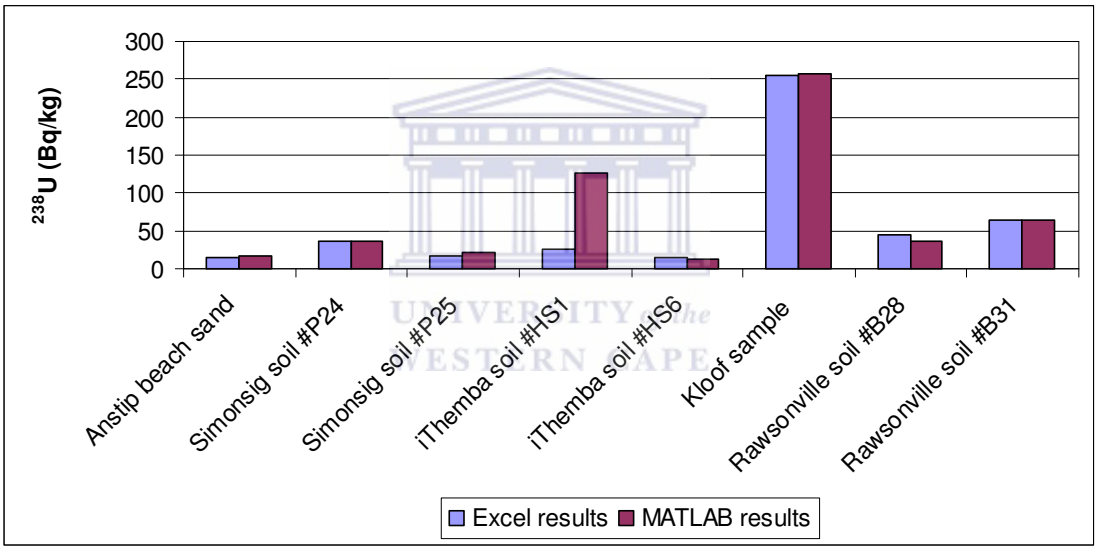

Figure 4.16: The comparison of the ^{238}U activity concentrations for the eight different samples that were measured.

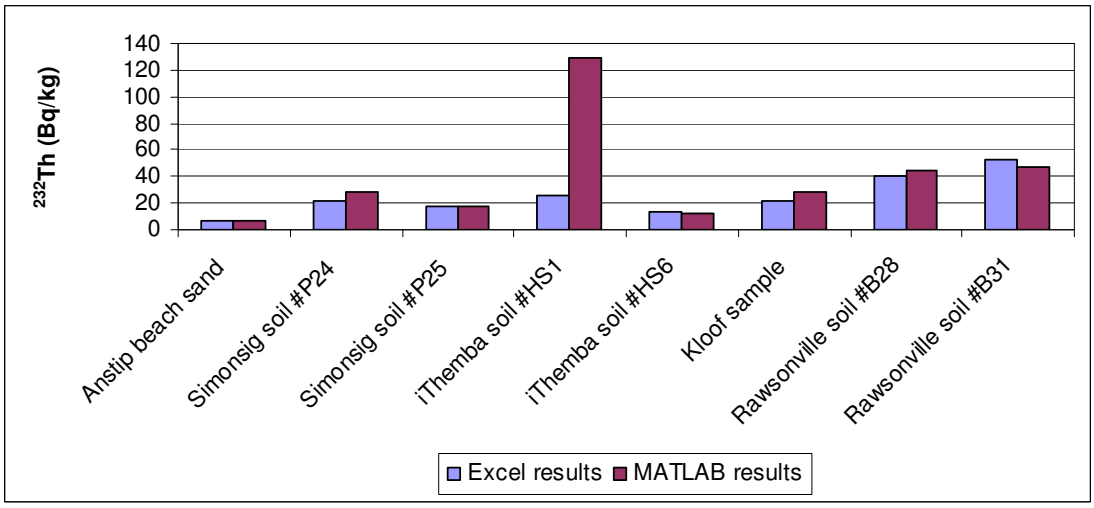

Figure 4.17: The comparison of the ^{232}Th activity concentrations for the eight different samples that were measured.

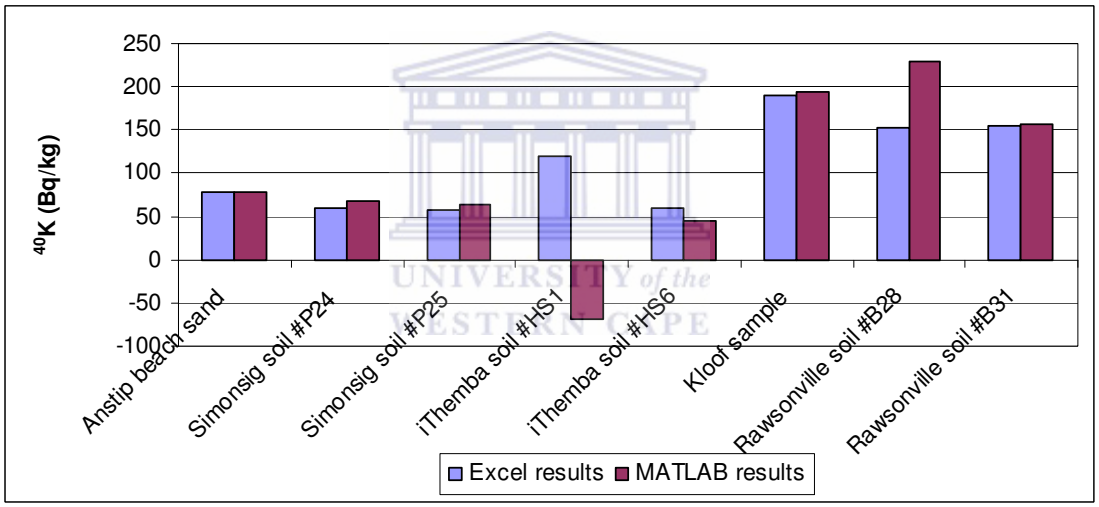

Figure 4.18: The comparison of the ^{40}K activity concentrations for the eight different samples that were measured.

4.5.2. Field measurements

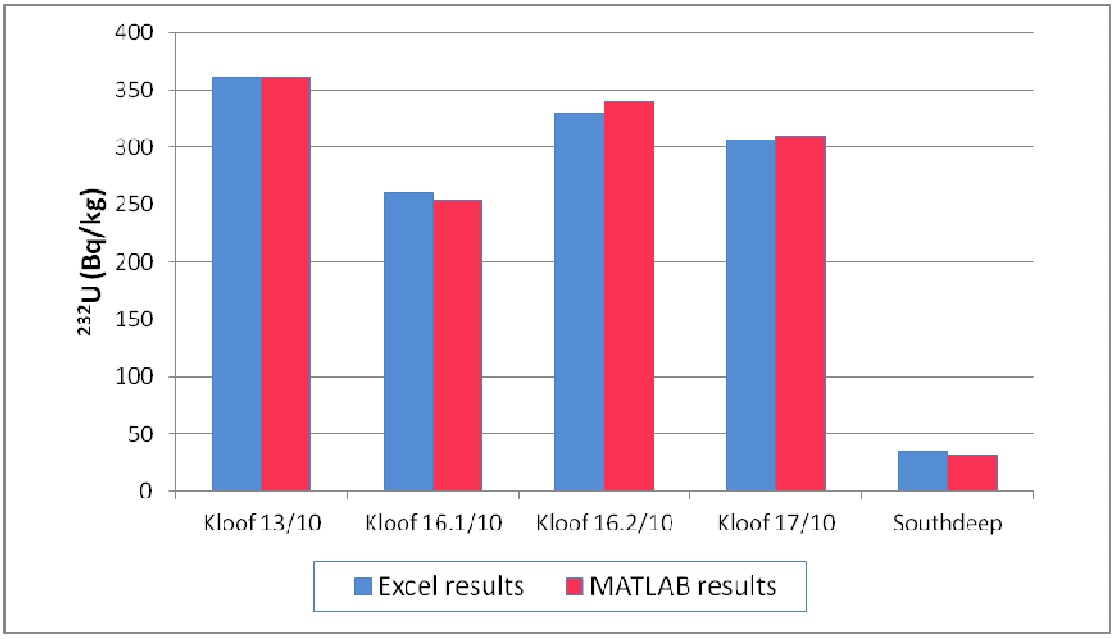

Figure 4.19: The comparison of the ^{238}U activity concentrations for the four Kloof stationary points and the one Southdeep stationary point.

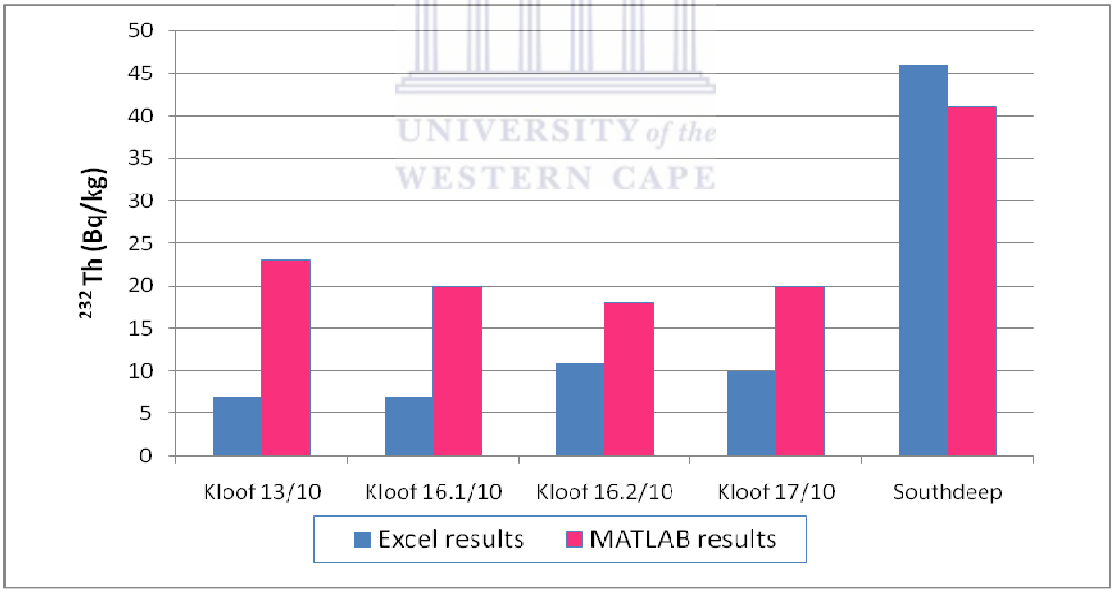

Figure 4.20: The comparison of the ^{232}Th activity concentrations for the four Kloof stationary points and the one Southdeep stationary point.

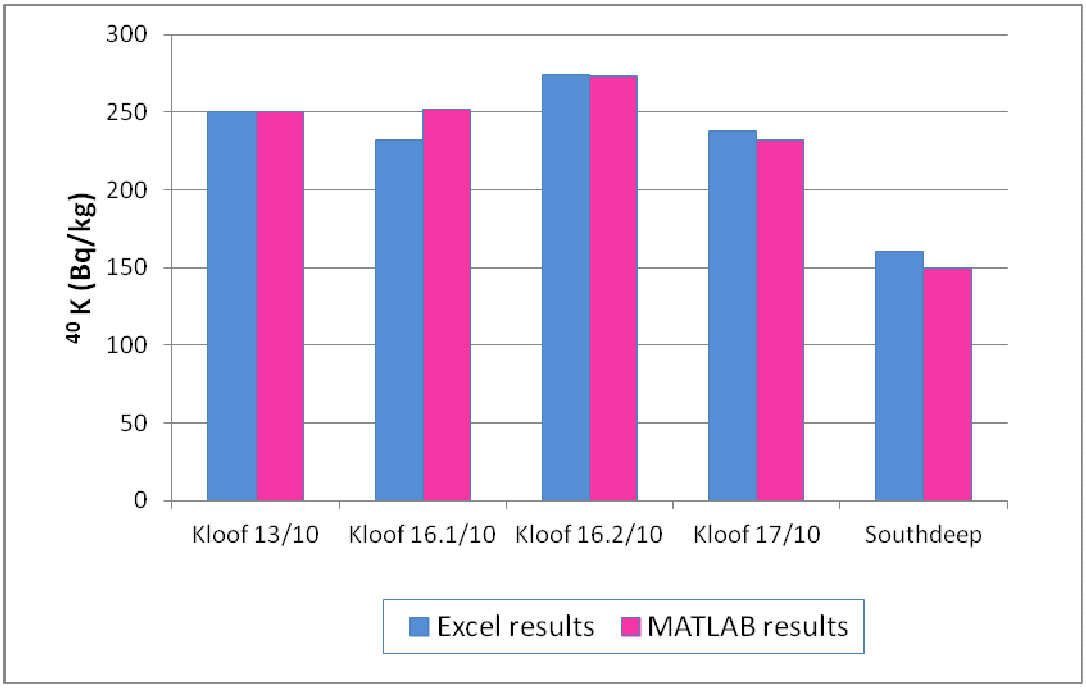

Figure 4.21: The comparison of the ^{40}K activity concentrations for the four Kloof stationary points and the one Southdeep stationary point.

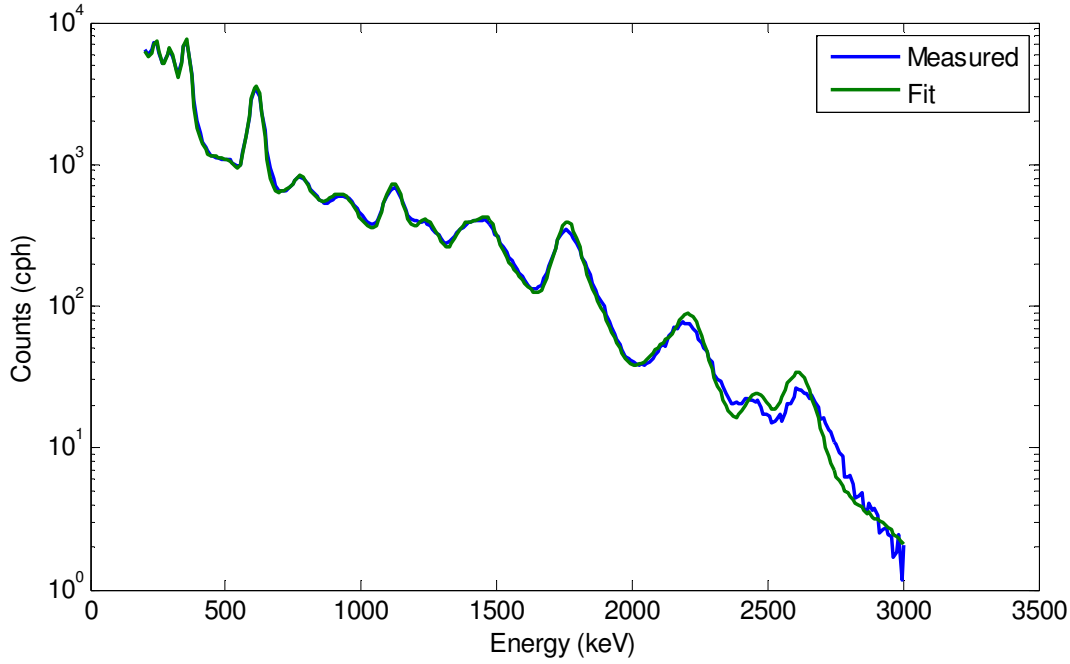

Figure 4.22: A background subtracted spectrum of the Kloof sample with the fitted spectrum using MATLAB for energies from 105 keV to 3005 keV.

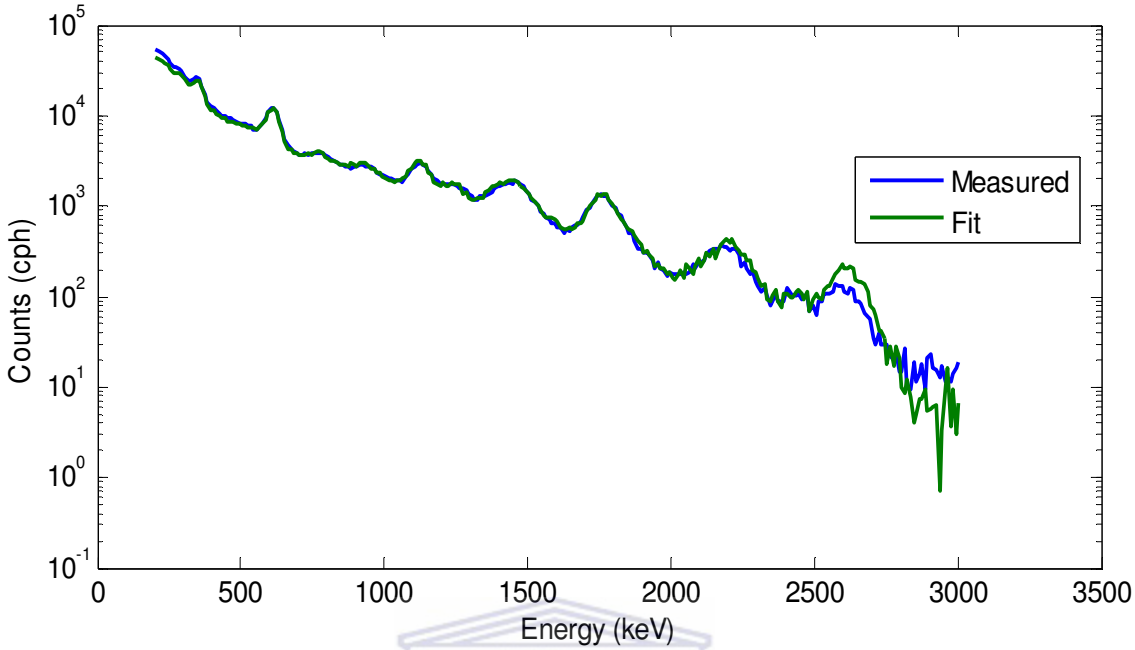

Figure 4.23: A spectrum measured on the stationary point Kloof 16.1/10 with the fitted spectrum using MATLAB for energies from 205 keV to 3005 keV.

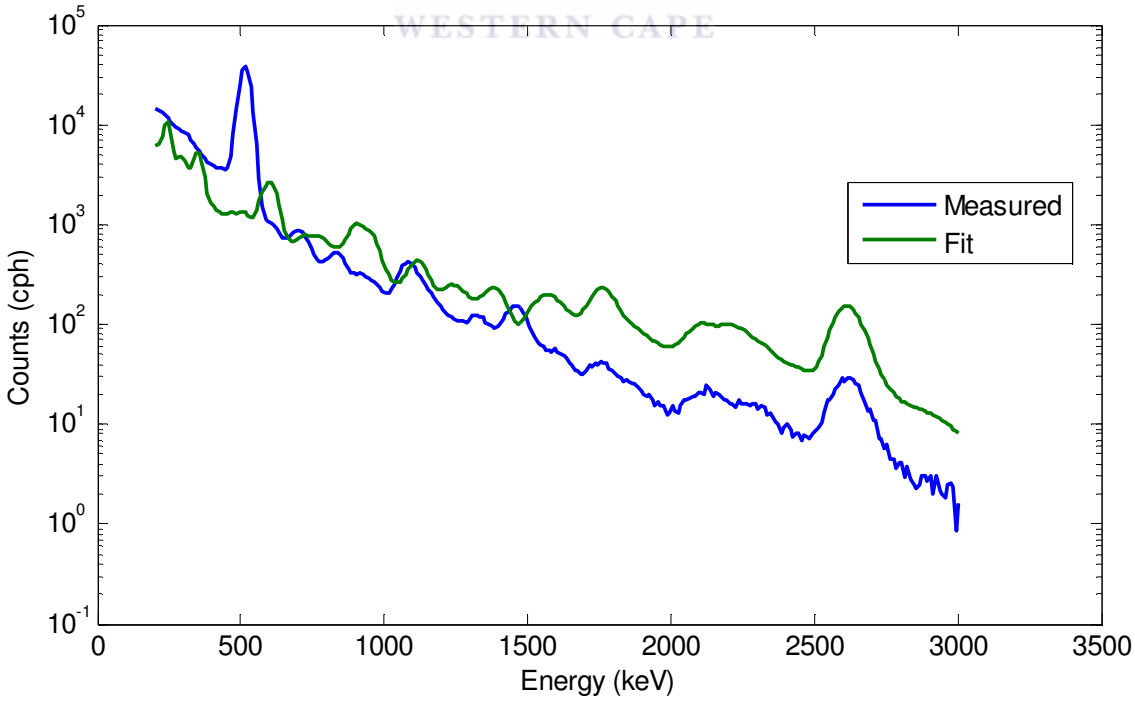

Figure 4.24: A background subtracted spectrum of the iThemba soil #HS1 sample with the fitted spectrum using MATLAB for energies from 105 keV to 3005 keV.

4.6 Discussion of the results

4.6.1 Laboratory Results

Activity concentrations of three different nuclei were extracted in each sample using the FSA method. A method where three standard spectra were added together multiplied by three coefficients and then fitted to the sample spectra. The best fit is achieved by choosing the best coefficients which ultimately represent the activity concentrations of nuclei in question by finding the minimum χ^2. Microsoft Excel was used manually to guess these coefficients until suitable ones are obtained using the fit visually and the χ^2. The MATLAB program was also used where built-in routines obtains the best coefficient for a minimum χ^2 and also produces error estimates on the estimated coefficients.

Comparing the overall results in tables 4.1 and 4.2, one can safely conclude that there is a good correlation between the Excel results and the MATLAB results. However there are some cases where there is a noticeable disparity between the two results especially for the ^{40}K energy peak. This disparity can be attributed to calculated spectra which have a poor fit to the measured spectrum. There are many reasons why calculated spectra may fit poorly to the measured spectra. These include spectra from samples containing anthropogenic radionuclides, spectra with low counts but high background counts and spectra which are susceptible to spectral drift.

The two iThemba samples were found to contain some anthropogenic radionuclides. The iThemba HS sample in particular contained very high counts from ^{22}Na ^{68}Ga and ^{54}Mn. These radionuclides are usually found in some locations in iThemba soil where they are discarded from the Isotope production division [Hla07]. The spectra that contains these anthropogenic radionuclides are particular difficult to fit in MATLAB as can be seen in figure 4.6. This is because unlike in Excel, in MATLAB you cannot manually fit the peaks which are of interests to you and leave the rest. In MATLAB the program attempts to fit all the peaks including the continuum as it can not differentiate between the anthropogenic and terrestrial peaks. This makes the MATLAB predictions totally unreliable in this instance, as can be seen in figure 4.24. The obviously poor fit when anthropogenic nuclei are present, indicates that the presence of such radionuclei will be easy to spot.

The NaI (Tl) detector is also known to be susceptible to spectral drifts. Figure 4.4 and figure 4.8 show two examples of such spectra where the shift in the measured spectrum makes it difficult to fit using the standard spectra. The 1461 keV line from ^{40}K and the 2614 keV line from ^{208}Tl showed clear evidence of drifts and consequently their peaks were broadened. This broadening of peaks also contributes to the formation of wider Compton scattering peaks that makes it difficult to fit other peaks like the 1120 keV, 1764 keV and 2204 keV ^{214}Bi peaks. The other problem associated with this spectral drift is that in some cases even though the calculated peaks may fit the measured peaks, the measured peaks are broader and some counts will be outside the fitted peaks and may be accidently omitted.

In practise when measuring natural radiation in soil and sand samples low count rates are expected. Sometimes the measured counts may be lower than the background counts. This results in poor fits of the standard spectra to the measured spectrum and

can lead to big uncertainties which lead to the disparities in the results, especially since the background counts also depend on the sample. In this study tap water was used to measure the background counts. The difference in density between tap water and the soil samples is an issue, as the gamma attenuation of the two is not the same. The gamma rays from the background radiation will be absorbed more by the soil samples than tap water. This results in a slightly higher background measurement in tap water than in soil samples. Subtracting this high background measurement from a less active sample could result in negative readings and a poor fit to the measured spectrum.

The difference in density between the different samples to the standard spectra was also a major factor that contributes to the disparity in the Excel and MATLAB results. When two spectra from samples of different densities are fitted one on top of the other, it is likely that their peak to Compton ratio will not fit perfectly as shown in figure 4.25. This phenomenon is caused by the difference in the self absorption of the sample. A less dense sample is likely to have a sharp photopeak with small counts in the continuum, whereas a denser sample is likely to have more counts in the continuum and fewer counts in the photopeak than a less dense sample as is the case in figure 4.25. This is because a gamma ray travelling in the denser sample has more probability of not depositing its full energy to the detector as it is more likely to be Compton scattered in the sample before it reaches the detector.

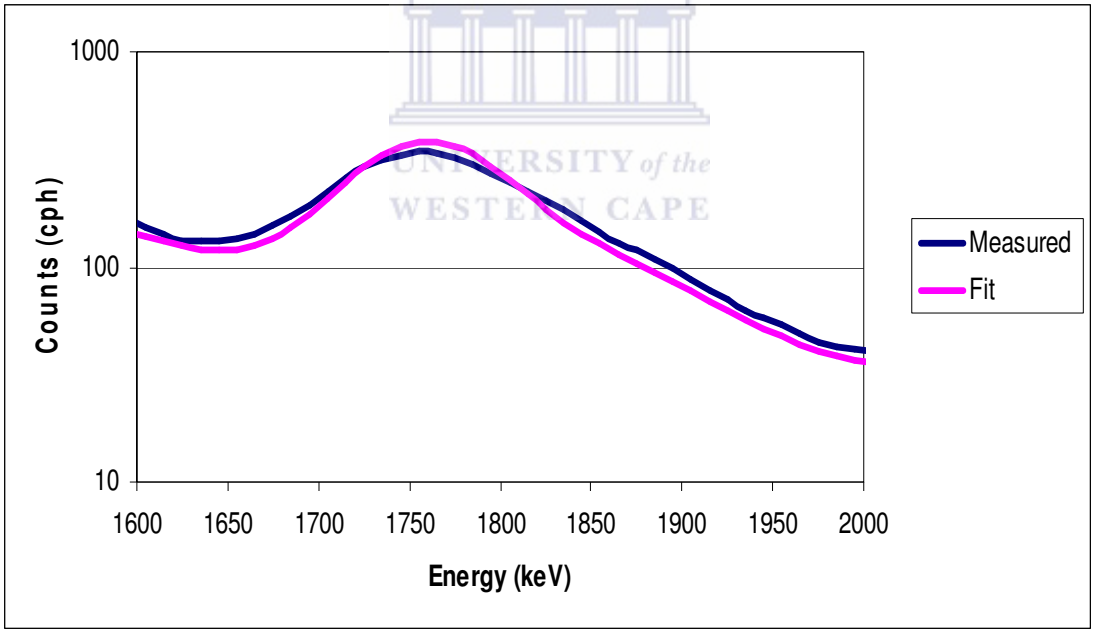

Figure 4.25: A figure showing the fitted spectrum to a measured spectrum of the Kloof sample around the1764 keV ^{214}Bi energy peak.

The situation that has been explained above tends to contribute to the disparity of the results because of the difference in the way the activity concentration values are extracted by the two methods. In Excel the standard spectra will be manually fitted to the photopeaks of the prominent peaks of the measured spectrum. The best fit will then be used to determine the activity concentrations. Whilst in MATLAB the whole spectrum including the continuum is recognised as important. The standard spectrum corresponding to the nuclide which has the lowest activity, will then often be wrongly

fitted since its activity will be changed to improve the fit to the continuum part of the measured spectrum as shown in figure 4.25. This artificial fit to the continuum will result in a poor fit to the peaks corresponding to this radionuclide, e.g. the automated fit to the Kloof data overestimates the fit to the 2614 keV ^{232}Th peak. This is done by the automated routine to improve the fit in the continuum. Figure 4.23 shows an example of an overestimate to the 2614 keV ^{232}Th peak because of the reasons stated above.

4.5.2 Field results

The field measurements from the Kloof mine dump showed good correlation between the Excel and MATLAB results. Since the measurements were done for a much shorter period than the laboratory measurements, there was not much time for spectral drifts. There were also no anthropogenic radionuclides in the soil. However there were higher values of ^{232}Th found in the MATLAB results compared to the Excel values because of the overestimation problem by MATLAB that is explained in section 4.5.1. The ^{232}Th values are also associated with high uncertainty values in both Excel and MATLAB measurements as the low counts in the ^{232}Th peak makes it difficult to fit. The background in the field measurement was not subtracted as it largely due to cosmic rays and we assume its contribution is small and does not contain peaks. The standard spectra include a fairly similar background since these spectra were measured at Lanseria, not too far from the Kloof mine. This does not mean the background is not treated properly as it is present in all three standard spectra. This does not seem to be a problem in the Kloof data where the counts are large, but will possibly be a problem in low activity areas.

Chapter 5 Conclusion and Outlook

This chapter summarizes the major discussion points in this study and the results achieved. It also gives some recommendation on problems faced and interesting future projects which can be done.

A highly efficient NaI detector was used to study activity concentrations of various samples containing natural radionulcides from different places. The detector proved to have enough efficiency to measure low levels of natural radiation coming from soil and sand samples which usually do not have very high levels of radiation. The detector also had good enough resolution to produce a spectrum which has separable peaks. All the important peaks for ^{238}U (such as the 1764 keV ^{214}Bi peak), ^{232}Th (such as the 2615 keV ^{208}Tl peak) and the 1461 keV ^{40}K peak were easily identifiable. The FWHM was measured using a ^{137}Cs source and was found to be 7.8%, which is a reasonable enough value and close to that of the manufacture of 7.0% also using a ^{137}Cs source.

The laboratory measurements were done in room 147b in the physics department at UWC. The NaI detector and the sample were positioned inside a lead castle to minimize the effect of background radiation from the walls, the floor and other types of background radiation like radon flux in the room and cosmic radiation. The NaI detector is known to also contain some residual radiation of U, Th, and K in its PMT which limits its sensitivity [The03]. Lead blocks were placed below the castle as the detector was exposed at the bottom. These lead blocks reduced the background count rate by about 20%. Tap water inside a Marinelli beaker was used to measure the background radiation. Since the density of water and its composition is different to that of sand or soil we believe that the background radiation traversed through water more easily than it does through sand or soil. This then causes a higher background reading in water than in sand and soil samples, therefore the background may have higher readings at the ^{40}K and ^{238}Th peaks than a low level sample. This makes it difficult to measure very low activity samples with the FSA method after background subtraction. A lead castle system which allows less background radiation is recommended for future measurements.

The NaI detector is known to be prone to spectral energy drift caused mainly by temperature changes inside and around the detector. An investigation was done to look at the spectral drift of this detector at room temperature. Hourly measured measurements of the centroid of a ^{137}Cs peak and room temperature were done. The centroid shifted about 4 keV from the minimum to the maximum channel; this is enough to disturb the fitting of standard spectra to the measured spectra when using the FSA method. The room temperature difference between the minimum and maximum temperature was 1.56 ºC. No correlation was found between the room temperature and the centroid shift. This means that temperature differences inside the detector could be more significant than room temperature changes. Many people have different solutions to this problem; from developing a technique that compensates for the temperature dependence of the light output [Lan09] to a more mathematical way of re establishing the centroid value for a fixed energy versus channel number relation [Sta97]. These and other methods may be considered for future studies.

Eight samples were measured using the FSA method with the NaI detector. The FSA method uses almost the whole spectrum as compared to the WA method and a least squares analysis method to determine the activity concentration of ^{238}U, ^{232}Th and ^{40}K radionuclides. The measurements were counted for approximately 24 hours (except the iThemba soil #HS1 which was counted for 45 hours due to low activity) for better statistics.

The ^{238}U, ^{232}Th and ^{40}K values ranged from a minimum of 14 ± 1 to 256 ± 10 Bq/kg, 7 ± 1 to 53 ± 1 Bq/kg and 57 ± 11 to 190 ± 20 Bq/kg respectively. The Kloof sample was the most active in ^{238}U and ^{40}K as expected from a sample from a Goldfields mine dump. The Rawsonville sample was the most active in ^{232}Th. The soil samples from iThemba contained some anthropogenic radionuclides like ^{22}Na, ^{68}Ga and ^{54}Mn which made it very difficult to fit [Hla07].

Activity concentration measurements were also done in-situ at the Kloof mine dumps. These measurements were done using the same portable NaI (Tl) detector that was used for lab measurements. Activity concentration values at Kloof ranged from 256 ± 10 to 360 ± 4 Bq/kg for ^{238}U, 7 ± 5 to 46 ± 7 Bq/kg for ^{232}Th and 230 ± 90 to 270 ± 180 Bq/kg for ^{40}K. The values that were obtained using Excel showed good correlation to those that were obtained using MATLAB as can be seen on the bar graphs in figure 4.19, 4.20 and 4.21. The Southdeep dump had very low levels of ^{238}U, (31 ± 2 Bq/kg) and ^{40}K (150 ± 17 Bq/kg) compared to Kloof. This was expected since Southdeep was not as yet used to dump mine tailings. The ^{232}Th content was higher in Southdeep than Kloof at 41 ± 2 Bq/kg.

The measurement techniques investigated in this thesis are important since they provide efficient methods to make measurements for radiation protection purposes. Using the dose coefficients 0.461, 0.623 and 0.0414 nGy/h per Bq/kg for ^{238}U, ^{232}Th and ^{40}K in soil respectively and converting nGy/h to mSv/y [Cot04], one can deduce the values for the maximum radiation exposure to a person who may stay on the Kloof mine dump for a year. Using the maximum values for the activity concentrations, the maximum radiation exposure will be 1.45 mSv for ^{238}U, 0.25 mSv for ^{232}Th and 0.10 mSv for ^{40}K. The value for ^{238}U is above the international standard of 1 mSv per year for the general public [www06], hence it will not be advisable for the general public to live on that mine dump especially with the possibility of radon (^{222}Rn) and radon daughter inhalation from one of the ^{238}U daughter nuclei. Further research is needed to investigate how radon will be dispersed in the air and how will it travel to reach people living close to the dump.

The FSA method combined with the NaI (Tl) detector proved to be a good method to use for activity concentration measurements of natural radiation both in laboratory and in the field as long as the radionuclides to be measured are known prior to the measurements and the standard spectra are available. The standard spectra can also be simulated using packages like MCNP and GEANT. In-situ measurements could be done using a portable NaI detection system in future to look at the activity concentration of natural radionuclides.

Appendices

Appendix A: Uncertainty calculations

An example of how the uncertainty values were calculated is shown here using the Rawsonville soil #B28 sample.

The following steps are taken when calculating the appropriate uncertainty value for each activity concentration of ^{238}U, ^{232}Th and ^{40}K.

1. Get the best values for the activity concentration using the linear squares fit method described in chapter 3 with the help of the plot of the measured spectrum and the calculated spectrum (fit).
2. Get the chi-squared value for the correct activity concentration values.
3. Change the activity concentration (by decreasing and then increasing the value) values until the chi-squared values changes by a calculated value for 95% confidence using the Excel worksheet (i.e. =confidence (alpha, standard deviation, size) where alpha is 0.05 for 95% confidence interval.
4. The difference between the best value for the each individual concentration and the value where the chi-squared value changes by the confidence value is then used as the uncertainty.

For all these calculation it has to be assumed that the channels are independent of each other, which is not necessarily the case.
Different values of activity concentrations with their respective chi-square values are shown in table 1-3 and the plots in figure 1-3. The best values for the activity concentrations are indicated in **bold** in the tables.

Table A.1: Activity concentration values for ^{238}U and their corresponding chi-squared values.

^{238}**Uconc (*Bq/kg*)**	χ^2
36	378.7
38	369.1
40	362.5
42	358.6
44	**357.5**
46	359.3
48	363.9
50	371.3
51	376.1

Table A.2: Activity concentration values for ^{232}Th and their corresponding chi-squared values.

^{232}Thconc (*Bq/kg*)	**χ^2**
35	382.6
36	375.2
37	368.9
38	363.9
39	360.2
40	**357.5**
42	355.9
44	359.0
46	367.0
48	379.6

Table A.3: Activity concentration values for ^{40}K and their corresponding chi-squared values.

^{232}Kconc (*Bq/kg*)	**χ^2**
102	375.8
120	368.2
130	364.5
140	361.2
153	**357.5**
200	350.0
250	351.8
280	357.6
300	363.5
320	371.0
331	375.8

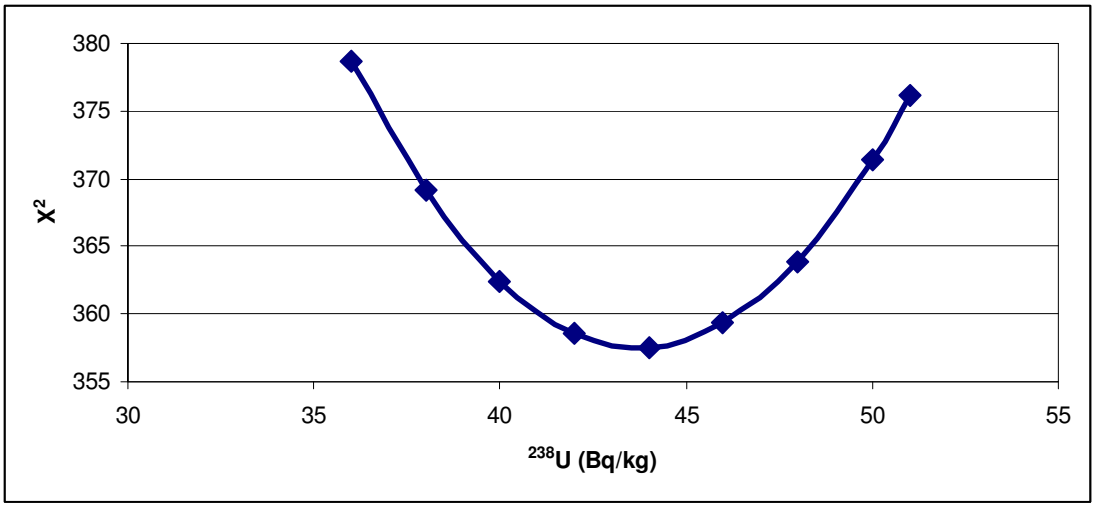

Figure A.1: A plot of different chi-squared values for varied activity concentrations of ^{238}U for the Rawsonville soil #B31 sample.

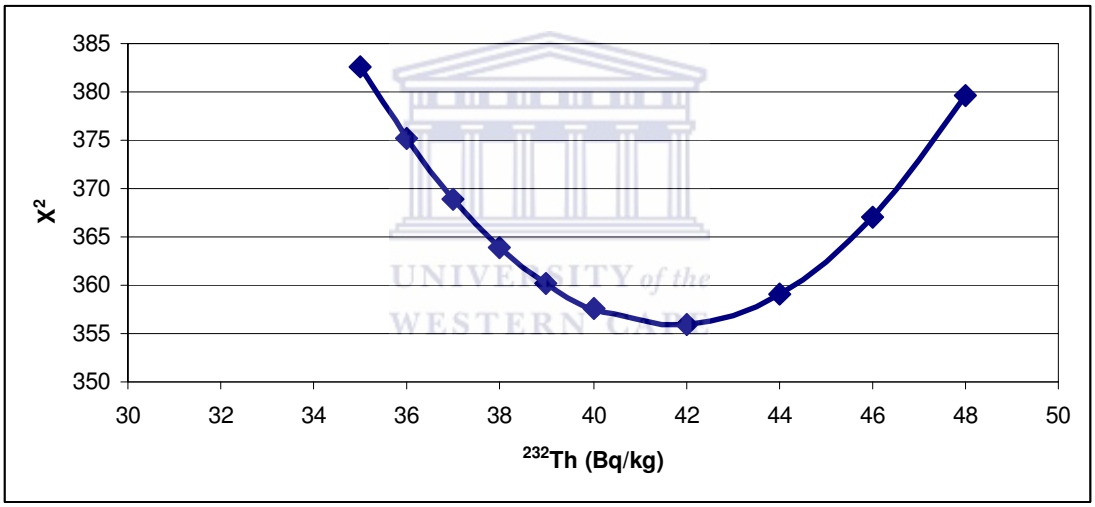

Figure A.2: A plot of different chi-square values for varied activity concentrations of ^{232}Th for the Rawsonville soil #B31 sample.

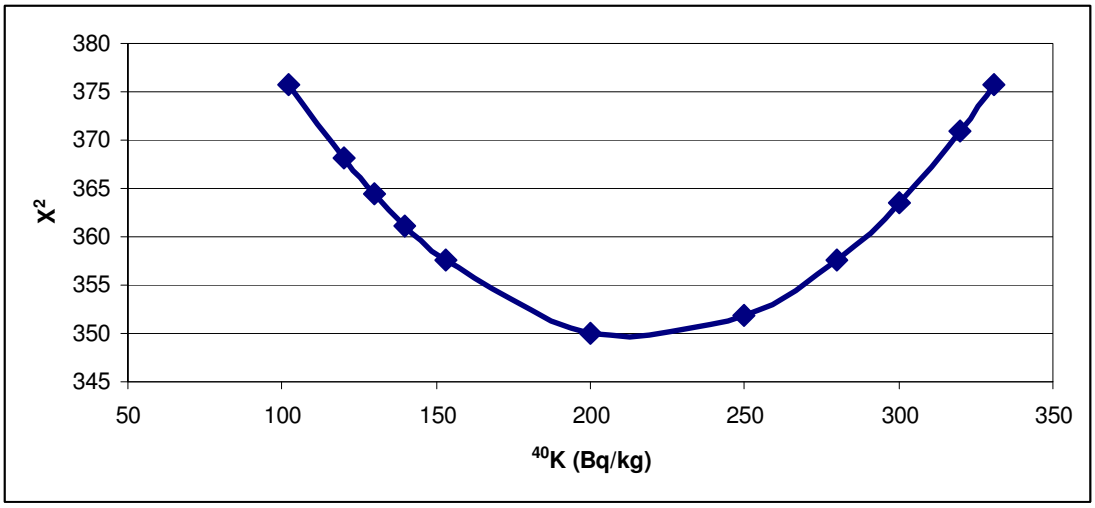

Figure A.3: A plot of different chi-square values for varied activity concentrations of ^{40}K for the Rawsonville soil #B31 sample.

When using this method for the uncertainty only the lower bound (from the best value down to the value where chi-square changes by the confidence factor) value is used since the upper one gives us a false reading as the fit moves up it leaves a 'tail' behind which still fits the measured spectrum hence it takes long for the chi-square value to change. The upper bound is used only if it is seen as 'reasonable'.

N.B: Sometimes the estimate with the lowest chi-squared value is not considered if it does not provide a reasonable fit, also because of the fact that the covariance is not taken into consideration.

Appendix B: Visual Basic programs

N.B. *Comments are in italics and green.*

Program 1: For arranging counts which are imported as 127 rows and 8 columns, to one column in excel.

```
Private Sub CommandButton1_Click()
'Declaring variables to be used in the programme
Dim Strings As String
Dim i As Integer
Dim j As Integer
Dim k As Integer
Dim l As Integer

Dim ResultCounter As Integer

k = Application.InputBox("Enter the value of k")
'k is the number corresponding to the first row location
l = Application.InputBox("Enter the value of l")
'l is the number corresponding to the first last location

  i = 1    'i is the first value of every row
  j = 8    'j is the last value of every row

  ResultCounter = k - 1    'Result counter is where the value must go after every iteration


                For k = k To l
'For loop that iterates from k to l

                  For i = i To j
 'For loop that iterates from i to j and the goes back to the bigger for loop for the next row.

 Worksheets("kloof-13-10R").Cells(ResultCounter, 14) =
Worksheets("kloof-13-10R").Cells(k, i).Value
 '   A line which shows to which cell the value should go every time after an iteration

    ResultCounter = ResultCounter + 1 'The loop must do another iteration until j

 Next
   '    The first loop terminates at j=8


  Next
'   The second loop terminates at j=8 of l
End Sub
```

Program 2: Program to rebinn the spectrum do that 1 channel is equal to 5 keV.

```
Private Sub CommandButton1_Click()
' Declaring varaibles
Dim Spectrum(110000)
Dim RebinSpectrum(100000)
Dim k As Integer
Dim m As Integer
Dim c1 As Integer
Dim c2 As Integer
Dim r0 As Integer
Dim ResultCounter As Integer

' Input the values from the spreadsheet
 r0 = Application.InputBox("Enter the value of r0") 'r0 is the initial row for the counts
      x = Application.InputBox("Enter the value of x") 'x is the row where counts and energy values will be place
      b = Application.InputBox("Enter the value of b") 'b is the constant term
       c = Application.InputBox("Enter the value of c") 'c is the linear coefficient
       d = Application.InputBox("Enter the value of d") 'd is the quadratic coefficient
' re-bin in steps of 10 kev, start at 10-20 and call this 15keV
estep = 10
' Start a for loop that counts from the first r0 to the last
  For ResultCounter = r0 To r0 + 1024
     Spectrum(ResultCounter - x) = Worksheets("kcl-07-02rr").Cells(ResultCounter, 14)
  Next ResultCounter
     'Start a for loop that places counts in bins of energies instead of channels
    For k = 1 To 420

      E1 = k * estep        'read the first k which makes E1 the first energy bin to be 15 keV
      E2 = E1 + estep       ' the second energy bin will be 15+10=25 keV
     'If its a linear function use the equation below
      If b = 0 Then
      ch1 = (E1 - d) / c
      ch2 = (E2 - d) / c
      Else
      'otherwise use quadratic equation to get Channels corresponding to E1 and E2
      ch1 = (-c + Sqr(c * c - 4 * b * (d - E1))) / (2 * b)
      ch2 = (-c + Sqr(c * c - 4 * b * (d - E2))) / (2 * b)
      End If

      c1 = (ch1 + 0.5)    'channels bigger than 0.5 are renamed as c1
      c2 = (ch2 - 0.5)    'channels smaller than 0.5 are renamed as c1

       'Counts which fall below a certain value of c1 are placed here
      RebinSpectrum(k) = (c1 - ch1) * Spectrum(c1 - 1)

        'Counts which fall in-between c1 and c2 are placed here
        For m = c1 To c2 - 1
        RebinSpectrum(k) = RebinSpectrum(k) + Spectrum(m)
```

```
            Next m
            'Counts which fall above c2 are placed here
            RebinSpectrum(k) = RebinSpectrum(k) + (ch2 - c2) * Spectrum(c2)


        'place energy values from row x up to the last k in column 19
        Worksheets("kcl-07-02rr").Cells(x + k, 19) = (k * 10) + 5
        'place counts from row x up to the last k in column 20
        Worksheets("kcl-07-02rr").Cells(x + k, 20) = RebinSpectrum(k)
    Next k
    'Iterate till the last k then stop

End Sub
```

Appendix C: Matlab program

A program for calculating activity concentrations using Matlab.

```
%%%%%%%%%%% Reading values from Excel spreadsheet%%%%%%%%%%%%%%
Energy = xlsread('ithemba1.xls', 1, 'C27:C307');
BG = xlsread('ithemba1.xls', 1, 'D27:D307');
Th = xlsread('ithemba1.xls', 1, 'E27:E307');
U = xlsread('ithemba1.xls', 1, 'F27:F307');
K = xlsread('ithemba1.xls', 1, 'G27:G307');
Sample = xlsread('ithemba1.xls', 1, 'H27:H307');
BGLT = xlsread('ithemba1.xls', 1, 'D5');
ThLT = xlsread('ithemba1.xls', 1, 'E5');
ULT = xlsread('ithemba1.xls', 1, 'F5');
KLT = xlsread('ithemba1.xls', 1, 'G5');
SampleLT = xlsread('ithemba1.xls', 1, 'H5');
ThBq = xlsread('ithemba1.xls', 1, 'N4');
UBq = xlsread('ithemba1.xls', 1, 'N6');
KBq = xlsread('ithemba1.xls', 1, 'N5');
Thkg = xlsread('ithemba1.xls', 1, 'O4');
Ukg = xlsread('ithemba1.xls', 1, 'O6');
Kkg = xlsread('ithemba1.xls', 1, 'O5');
Samplekg =xlsread('ithemba1.xls',1,'O7');
%%%%%%%%%%%%%%%Normalising the values by livetime and mass%%%%%%%%%%
BGval = BG/BGLT*3600;
Thval = Th/ThLT*3600/Thkg;
Uval = U/ULT*3600/Ukg;
Kval = K/KLT*3600/Kkg;
Sampleval = Sample/SampleLT*3600/Samplekg;
%%%%%%%%%%%%%%%%%%%%%%%%Normalising the values by activity concentration
%%%%%%%%%%%%%%%%%%%%%%%%and subtracting
%%%%%%%%%%%%%%%%%%%%%%%%background%%%%%%%%%%%%%%
Threal = (Thval - BGval)/ThBq;
Ureal = (Uval - BGval)/UBq;
Kreal = (Kval - BGval)/KBq;
Samplereal  = Sampleval - BGval;
y = Samplereal;   %declaring y as my normalised vector for the measured spectrum%
beta0 = [1;1;1];    %declaring initial guesses for the activity concentration as beta0
X = [Threal Ureal Kreal]; %declaring my counts as a matrix x
options = statset('Robust','on','Tune',1,'WgtFun',@wfun)
%weighting the counts for a better fit
 [beta,resid,J,Sigma] = nlinfit(X,y,@myfun,beta0) %acquiring activity concentrations as beta
ci = nlparci(beta,resid,J)  %produce errors on activity concentrations
plot(Energy,y,Energy,X*beta) %plot the measured and fitted spectra
%%%%%%%%%%%%%Calculation of the variance sigma^2%%%%%%%%%%%
sigma = ((x(1)/(ThBq*Thkg)^2))*(Th/(ThLT)^2) + ((x(2)/(UBq*Ukg)^2))*(U/(ULT)^2)
 + ((x(3)/(KBq*Kkg)^2))*(K/(KLT)^2) + (Sample/(SampleLT*Samplekg)^2)
 + (BG/(BGLT)^2)*(1+(x(1)/ThBq)^2+(x(2)/UBq)^2+(x(3)/KBq)^2);
sigma1 = sigma*3600^2;
%%%%%%%%%%%%%%%%%%%%%%%%%%%%%%%%%%%%%%%%%%%%%%%%%%%%%%%%%%%%%%%
```

```
%%%%%%%%%The for loop for calculating the chi-squared value%%%%%%%%
chi = 0
for n = 1:281
    chi = chi+(y(n)-(x(n,1)*beta(1)+x(n,2)*beta(2)+x(n,3)*beta(3)))/(sigma1(n))^0.5;
end
chi = (chi'*chi)/280
%%%%%%%%%%%%%%%%%%%%%%%%%%%%%%%%%%%%%%%%%%%%%%%%%%%%%%%%%%%%%%%%
%%%%The function used to calculate the estimated coefficients beta which represents the
activity concentrations, y being the vector containing the measured spectrum and x
representing the standard spectra%%%%%%%%%%%%%%%%%%%%%%%%%%%%%%%

function y = myfun(beta,x)
y = x*beta;
%%%%%%%%%%The function that introduces the
weights%%%%%%%%%%%%%%%%%%%%%%%%%%%%%%%%%%%%%%%%%%%%%%%%%%%%%%%%

function w = wfun(~)
global sigma1
w=1./sigma1;
end
%%%%%%%%%%%%%%%%%%%%%%%%%%%%%%%%%%%%%%%%%%%%%%%%%%%%%%%%%%%%%%%%
```

References

[Ame00] Amersham QSA catalogue (2000).

[Cot04] Coto N.R., *"Environmental radiation measurements at Koeberg Nuclear Power Station using Electret Ion Chambers"*. University of the Western-Cape (RSA), Unpublished Msc. Thesis (2004)

[Dam05] Damon R.W., *"Determination of the photopeak detection efficiency of a HPGe detector, for volume sources, via Monte Carlo simulations"*. University of the Western-Cape (RSA), Unpublished Msc. Thesis (2005)

[Dem98] De Meijer R.J., *"Heavy Minerals: From 'Edelstein' to Einstein"*, J. Geochemical Exploration 62, 88 (1998).

[Eva55] Evans R.D., *"The Atomic Nucleus"*, McGraw-Hill, New York, (1955).

[Gil95] Gilmore G., Hemingway J.D, *"Practical Gamma-ray spectrometer"*, John Wiley & Sons, New York (1995).

[Hen01] Hendriks P.H.G.M., *"Full spectrum analysis of natural γ ray spectra"*, Journal of Environmental Radioactivity 53 (2001), pp. 365.

[Hen03] Hendricks P. *"In depth γ-ray studies" Borehole Measurements,* Rijksuniversiteit Groningen, Published, PhD Thesis (2003).

[Hla07] Hlatshwayo I.N., *"In-situ gamma ray mapping of environmental radioactivity at Ithemba labs and associated risk assessment"*. University of Zululand (RSA), Unpublished Msc. Thesis (2007)

[Kno00] Knoll G.F., *"Radiation detection and Measurements"*, third edition John Wiles & Sons, New York, (2000).

[Kra83] Krane K.S., "*Modern Physics"*, John Wiley & Sons Inc, New York (1983)

[Kra88] Krane K.S., *"Introductory Nuclear Physics"*, John Wiley & Sons Inc, New York, 10158 (1988).

[Lan09] Lanakiev K.D., Alexandrov B.S., Littlewood P.B., Browne M.C., *"Temperature behaviour of NaI(Tl) scintillation detectors"*. Nuclear Instrument and Methods in Physics Research A 49640 (2009)

[Lap72] Lapp R.E, Andrews H.L., *"Nuclear Radiation Physics"* fourth edition, Prentice-Hall Inc., Englewood Cliffs, New Jersey (1972)

[Lav96] Lavi N.,Alfassi Z.B., Drndarski N., *"Calibration of Marinelli vessels*

for measurement of radioactive environmental samples". Nuclear and Methods in Physics Research A 385 (1997) 376-380

[Leo87] Leo W.R., *"Techniques for nuclear and particle physics experiments"*, Springer-Verlag Berlin (1987).

[Lil01] Lilley J., "*Nuclear physics, Principles and Applications"*, John Wiley & Sons, New York (2001).

[Lin04] Lindsay R., de Meijer R.J.,Joseph A.D., Motlhabane T.G.K., Newman R.T., Tsela S.A., Speelman W.J., *"Measurement of radon exhalation from a gold mine tailings dam by γ ray mapping."* Radiation physics and chemistry 71 (2004) 797 - 798

[Map04] Maphoto K.P., *"Determination of Natural Radioactivity concentrations in soil: a comparative study of Windows and Full Spectrum Analysis"*, University of the Western-Cape (RSA), Unpublished Msc. Thesis (2004)

[Mos06] Moszyński M., Nassalski A., Syntfeld-Każuch A., Szczęśniak T., Czarnicki W., Wolski D., Pausch G. Stein J., *"Temperature dependence of LaBr3(Ce), LaCl3(Ce) and NaI(Tl) scintillators."* Nuclear Instruments and Methods in Physics Research A 568 (2006) 739-751.

[Mba07] Mbatha N.B, *"Radiometric study of beach sand deposits along the coast of Western Cape province, South Africa."*. University of the Western-Cape (RSA), Unpublished MSc. Thesis (2007).

[New08] Newman R.T., Lindsay R., Maphoto K.P., Mohanty A.K., Mlwilo N.A., Roux G.D.,de Meijer R.J., Hlatshwayo I.N., *"Determination of soil, sand and ore primordial radionuclide concentrations by full-spectrum analyses of high-purity germanium detector spectra"*. Applied Radiation and Isotopes 66, 855-899 (2008)

[RL148] *.Preparation and Certification of IAEA Gamma Spectrometry Reference Materials.* RGU-1, RGTh-1 and RGK-1, AQCS Intercomparison Runs Reference materials, IAEA.

[Rob09] Robinson S.M., Kiff S.D., Ashbaker E.D., Flunerfelt E., Salvitti M., *"Effects of high count rate and gain shift on isotope-identification algorithms"* Nuclear Instruments an Methods in Physics Research A 610 (2009) 509-514.

[Spe04] Speelman W.J., *"Modelling and measuring of radon diffusion through soil for application in mine tailings dams"*. University of the Western-Cape (RSA), Unpublished MSc. Thesis (2004).

[Sta97] Stapel C., Lumberg J., De Meijer R.J., *"Calibration of BGO scintillation detectors in a bore-hole geometry"*. Nuclear Geophysics Division (NGD), Rijksuniversiteit Groningen, Internal report Z62 (1997).

[The03] Theordosson P., *"K/Th/U in photomultiplier tubes and improved low-level NaI detectors"*. Nuclear Instruments and Methods in Physics Research A 506 (2003) 143–148

[www01] www.southafrica.info/business/economy/sectors/mining taken on 15/07/2010

[www02] www.medusa-online.com/en/ taken on 15/11/2011

[www03] www.icx-radiation.de taken on 23/11/2011

[www04] www.mathworks.com/products/matlab taken on 22/11/2011

[www05] www.six-sigma-material.com/Confidence -Interval taken on 07/07/2011

[www06] www.iaea.org/Publications/Factsheets/English/radlife.html taken on 21/02/2012